www.gecarbon.org

# BOLETIN del Grupo Español del Carbón

ISSN 2172 - 6094
nº 61/ Septiembre 2021

INDICE

Editorial .....1

Metodolgías innovadoras para la fabricación de andamios basados en polímeros conductores y nanotubos de carbono para aplicaciones biomédicas .....2

Nuevos avances sobre la evolución de la química superficial del soporte durante la preparación de catalizadores óxido metálico-carbón activado mediante impregnación húmeda convencional .....7

¿Podemos cribar sistemáticamente millones de estructuras químicas para una captura de carbono económica?.....14

Nanomateriales de carbono para holografía .....17

Nanomateriales de carbono para aplicaciones relacionadas con la piel .....25

BlackCycle: un gran proyecto europeo para reciclar neumáticos fuera de uso en neumáticos nuevos .....33



## Editorial

**Carbon-based research advances featuring young Spanish talents (2)**

En palabras del mismísimo Presidente de la Federación de Jóvenes Investigadores de este país, “cuando hablamos de jóvenes investigadores en España, estamos hablando de las mentes más formadas de cada rama del conocimiento”. Sí, un talento indudable, pero también unas condiciones de trabajo duras, unas expectativas de futuro muy oscuras, y un día a día que tiene que apoyarse en gran medida en una enorme vocación para poder sobrellevar las dificultades. No podemos negarlo, ser joven y dedicarse a la ciencia en este país es una profesión de riesgo. Y si entendemos como “joven” el hecho de ser menor de 40 años ya se ve dónde está el problema… Nos enfrentamos a problemas como la excesiva burocratización (que es de toda la ciencia, pero que castiga mucho más a l@s jóvenes), la falta de estabilidad o el envejecimiento de las plantillas sin apenas reposición, teniendo además que demostrar para ello muchísimo a cambio de muy poco… o nada. La solución de un problema debe comenzar irremediablemente por la identificación del mismo, y esto a su vez pasa por darle visibilidad. Por lo tanto, de nuevo, en este segundo número del “especial” dedicado a jóvenes que investigan en temáticas relacionadas con el carbono, se mostrarán excelentes trabajos que vuelven a poner de manifiesto la gran calidad que tienen los talentos que nacen en España, y que, a pesar de todas las dificultades, y del escaso reconocimiento institucional y/o gubernamental, aquí sigue habiendo excelentes mimbres que merecen un futuro acorde a su valía.

Así, en el presente número se recoge el trabajo de la Dra. Núria Alegret (CIC-BiomaGUNE), donde se revisan los últimos avances en andamiajes basados en nanotubos de carbono para aplicaciones biomédicas; también el trabajo del Dr. Adrián Barroso (Universidad de Salamanca), que presenta resultados de investigación en el campo de los catalizadores de óxidos metálicos soportados sobre carbón activado; el trabajo de la Dra. Susana García (RCCS; Heriot-Watt University, UK), donde se muestran herramientas computacionales para el cribado sistemático de materiales útiles en captura de $CO_2$; el trabajo de la Dra. María Isabel Lucío (Universidad Politécnica de Valencia), que revisa el estado del arte de materiales de carbono para holografía; y por último, y no menos importante, la revisión de la Dra. Cristina Martín (Universidad Carlos III de Madrid), que versa sobre nanomateriales de carbono para aplicaciones relacionadas con la piel.

La calidad de estas contribuciones (tal como sucedió en el número anterior) es, nuevamente, un ejemplo de lo mucho que l@s científic@s jóvenes españoles pueden (podemos) aportar a cualquier campo de la ciencia y la tecnología y, más en concreto, al campo de los materiales basados en carbono.

#materiales_de_carbono

#jóvenes_investigadores

#talento

#investigación_y_ciencia

José Miguel González
ICB-CSIC

# Innovate methodologies for manufacturing scaffolds based on conducting polymers and carbon nanotubes for biomedical applications

## Metodolgías innovadoras para la fabricación de andamios basados en polímeros conductores y nanotubos de carbono para aplicaciones biomédicas

**Antonio Dominguez-Alfaro[1], Nuria Alegret[1]***

*Center for Cooperative Research in Biomaterials (CIC biomaGUNE), Basque Research and Technology Alliance (BRTA), 20014 Donostia-San Sebastian, Spain*

**nalegret@cicbiomagune.es*

### Abstract

Since carbon nanotubes (CNTs) or conducting polymers (CPs) have been used in thin film for biomedical applications, the field have required the evolution to more real and complex matrices. 3D structures enhance effectivity and increase ratio/surface at the same time that provide complexity and heterogeneity of real systems. However, the manufacturing of structures composed of this two outstanding materials is still a challenged due to their poor processability. In fact, the general way to include one or both material is based on post-processing steps. In this review we presented conventional method based on fiber meshes, hydrogels, porous scaffold or post processing and non-conventional methods highlighted by the structure formation *in-situ* during the polymerization process. It is noteworthy remark that there are not many examples of the combination of both materials for the biomedical field, most of the examples reported in literature are focused in energy storage applications.

### Introduction

Up to date, applications in the biomedical field has been focused in the construction of bidimensional materials. However, this type of planar substrates does not provide the complexity and heterogeneity of real systems, therefore the formation of three-dimensional structures has turned essential for this field. Mainly, tridimensionality enhance effectivity and increase ratio/surface aspect at the same time that provide complexity and heterogeneity of real systems.[1][2]"

Particularly, tridimensionality has gain importance in applications ranging from sensor, tissue engineering and bioelectronics within the biomedical field. Tissue engineering is focused on the repair or replacement of damaged or diseased tissues with synthetic and/or natural implants. The conductive scaffolds must be biocompatible and reduce immune reactions of the body. Furthermore, the material should assist the adhesion and extension of cells while mimic the biological environment.[3–5] Therefore, scaffolds should provide suitable porosity, permeability and mechanical stability to mimic the biological environment.

Carbon nanotubes (CNTs) are considered 1D nanomaterials due to their nanoscale geometry formed by tubular and thin shape. Moreover, CNTs possess high electrical conductivity and high ratio weigh/strength that outstand it capabilities.[4] The manufacturing of 3D structures made uniquely of CNTs presents many drawbacks, mainly because

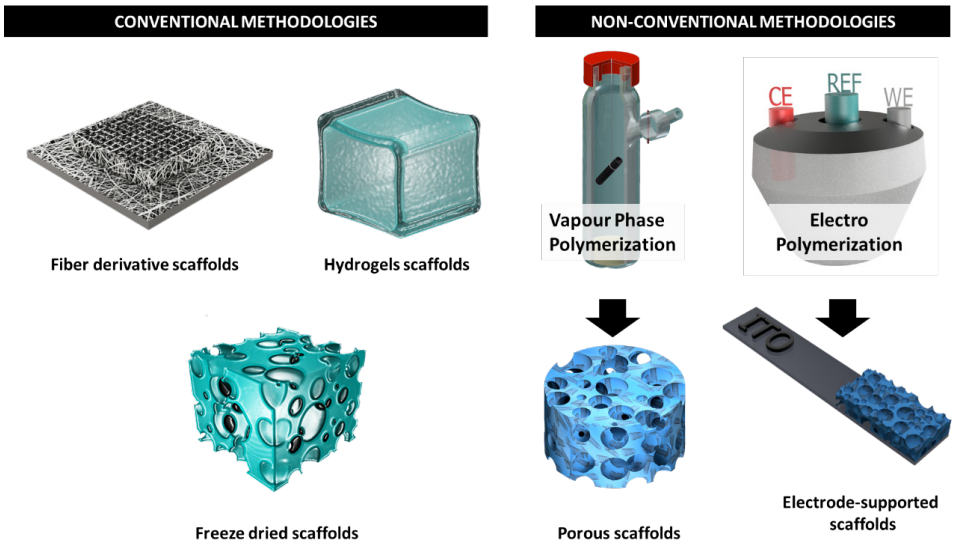


**Figure 1.** Schematic representation of the two main ways for the manufacturing of different materials composed of CNTs and CPs. Those methodologies can be divided in conventional and non-conventional methodologies.

their poor processability. Therefore, their combination with polymers represents a suitable option to make them more processable while maintain or even enhance properties such as conductivity and biocompatibility. In this line, the polymers that could confer these requirements are the conducting polymers. Poly pyrrole (PPy), polyaniline (PANI) and poly 3,4-ethylenedioxytiophene (PEDOT) are the most used polymer in the biomedical field because its high conductivity, biocompatibility, heterogeneity and chemical stability. CPs poses a positive charge when are oxidized, that is generally used for doping. The most representative example is PEDOT doped with polystyrene sulfonate (PSS), however it can be substitute by other electroactive or charged species, as carbon-based materials or biopolymers, among others.

The number of methodologies described for hybrids 3D scaffolds made of CNTs and CPs for biomedical applications are limited to fiber derivative methods, freeze-dried and hydrogel-synthesis methods. The materials that stands out are papers or fibers, foams and hydrogels. However, there are other non-conventional methods that engineer the CP polymerization within the tridimensional template. Basically, they are vapor phase polymerization (VPP) and electropolymerization (EP) that have not been explored in detail literature.

## 1. Conventional methodologies

### *1.1. Fiber-derivative scaffolds*

Fibers are tridimensional structures ranged from μm to mm size. There are two main methods for the manufacturing of meshes: paper-like composites and electrospinning. Fibers composed of PPy, CNTs and polyacrilonitrile (PAN) were prepared by electrospinning and investigate its biocompatibility with human keratinocytes *in vitro*. PPy concentration modulated the electrospun fiber and CNTs aggregates formed beads and disordered parts along the surface of nanofibers. The role in biocompatibility of the CNTs was studied comparing PAN/PPy and PAN/PPy/CNT scaffolds. Besides, both scaffolds presented good biocompatibility and provided adhesion and proliferation of keratinocytes. [6] PAN/PPy/MWCNT fibers were also used to modulate screen-printed carbon electrodes (SPCEs). In this case, CNT-embedded PAN electrospun with diameter above 200 nm were coated with a PPy *via* vapor-phase polymerization. The device was used for biosensing of glucose oxidase (GOX) without redox mediator with a limit of detection of 15.51 μM and a sensitivity of 5.41 A/mM·cm$^2$.[7]copolymer networks have been prepared sequentially by partially curing at low temperature followed by a final cure at high temperature. A single exothermic peak was observed in the differential scanning calorimetry (DSC Kobayashi *et al.* synthesized in a first step polyaniline/carbon nanotube (PANI/CNT) composite by oxidative method. Then they dispersed PANI/CNT material in poly (N-isopropyl acrylamide-co-methacrylic acid) (PNIPAm-co-MAA) and spinned at high voltage on an aluminum collector to forms three-dimensional (3D) fiber meshes. L929 fibroblasts was used to study the cellular response and cell viability at 7th day. The presence of the CNT enhance the cell viability of the scaffolds observed by calcein-AM and PI dye concluding their high suitability for tissue engineering applications.[8] On the other hand, Nayagan and coworkers manufactured densely paper-like scaffolds of aligned multiwalled carbon nanotubes embedded in a flexible and biocompatible block copolymer. The scaffold of 1 mm thickness was implanted intramuscularly were implanted in pairs in three locations of guinea pig's back, i.e. rostral, middle, and caudal along. They demonstrated that immobilization of multiwalled ACNTs did not incite a significant foreign-body reaction in post-chronic implantation. [9] In a next study, they developed a simple and economical method for making flexible electrodes by coating polypyrrole (PPy)–multiwalled carbon nanotube (CNT) composites on cellulose membranes. They used this bio-batteries concept, capable of working as dry body implants, which can be activated by the body fuids *in-vivo*. Various protein concentrations of bovine serum albumin (BSA) were applied as electrolytes in the system. The battery can be charged up to 35.1 hours (1.26 W h) in the protein-containing electrolyte.[10]

### *1.2. Freeze-dried scaffolds*

Freeze-dried are a common method used for this field due to most of the materials synthesized for biological purposed are synthesized in water. Therefore, water can be removed by freeze-dried/tawing cycles and generate porous materials. MWCNT/PEDOT:PSS with hierarchical microstructures was manufactured by freeze-drying method forming foam-like structures. Then, polydimethylsiloxane (PDMS) was introduced into the MWCNT/PEDOT:PSS foam to form a self-standing structure with thermally and electrically conductive.[11] There are many examples based on freeze-drying method subsequently after mixed, however most of them are not applied in the biomedical field. As exception, PEDOT:PSS/CNT mixture crosslinked with glycidoxypropyltrimethoxysilane (GOPS) to form porous scaffolds after freeze drying. Mechanical properties, porosity, biocompatibility and excellent conductivity rendered suitable for biosensing and monitoring applications. Alongside the enhancement in the electrical conductivity, the MWCNT-modified scaffolds exhibited good cytocompatibility and biofunctionalization (i.e., PLL) capability, important for biosensing and cell attachment (i.e., to promote adhesion of specific cell types). Overall, such high-performance systems can be useful for applications where electronic performance is particularly important, such as in applications for tissue stimulation and electronic implants.[12]

### *1.3. Hydrogels scaffolds*

Hydrogels can be synthesized via covalent crosslinking or supramolecular interactions. This type of materials is characterized because its softness, insulation and swelling capability.[3] Therefore, inclusion of CNTs and CP as fillers forms composite-like material with new properties. CNT was physically crosslinked with N-isopropylacrylamide (NIPAM), embedding PPy throughout an oxidative polymerization in a post-processing step. These hydrogels, also containing β-cyclodextrin (β-CD), exhibit high conductivity, self-healing properties, flexible and elastic mechanical properties and rapid stimuli-responsive properties both to temperature and near-infrared (NIR)-light. Moreover, cytotoxicity test with L929 fibroblast cells and C2C12 myoblast conclude it low toxicity. Taken together, these multifunctional hydrogels are excellent candidates for artificial organs.[13] In a third approach, oxidative cross-linking was employed to simultaneously include catechol-functionalized hyaluronic acid (HA–CA) with PPy and CNT to forms three-dimensional gels. This gels promote differentiation of human neural stem/progenitor cells (hNSPCs) and improve electrophysiological functionality compared to HA–CA hydrogel cells differentiated. The results suggest formation of mechanism for stem cell neurogenesis and pointed out as promising cell-culture platform for neuronal regeneration.[14]

## 2. Non-conventional methodologies

### *2.1. Vapour phase polymerization*

Vapor phase polymerization (VPP) of CPs was developed at the earliest of 2000 and is generally employed for the manufacturing of CP-thin films. As well as polymerization in solution, VPP is a chemical oxidative polymerization that use iron reagents. However, this technique presents limitation within the manufacturing of 3D structures due to the formation of oligomers that presents low reticulation degree and low mechanical properties. Hence, the use of nanocomposites is an alternative approach to form 3D structures. For example, 3D PEDOT-$SiO_2$ porous structure were synthesized *via* vapour phase polymerized in situ using polystyrene microparticles as template.[15] Besides SiO2, polyurethane fabricated sequentially gas foaming and vapor phase polymerization methods produce 3D flexible foams with biocompatibility evaluated by MC3T3-E1 cell culture along 7 days.[16]

In a first work carried out in our lab, VPP was modulated in order to obtain three-dimensional PPy/CNT scaffolds for neural prostheses candidate. Crystal sugar grains were used as sacrificial template which, in comparision with other proogens, sugar crystal grain are high friendly with biological applications. VPP method is very versatile as morphology, composition, porosity, mechanical properties and shape can be easily modulated throughout the reaction conditions. The composition, porosity and electrical conductivity confer C8-D1A astrocytic cell biocompatibility after 6 days of incubation.[17] Apart from PPy, the PEDOT polymerization is challenged because the polymerization rate and oligomerization. Proof of this, PEDOT scaffolds without CNT were not manufacture because collapsed easily. The presence of CNT gives more stability to the structure while very soft mechanical properties with Young's modulus ranged between 20 and 50 kPa. Scaffolds presented good biocompatibility at 3-6 days of C8-D1A astrocyte and very high cell attachment.[18]

### *2.2. Electrochemical polymerization*

While VPP requires the action of an oxidant for PEDOT polymerization, electropolymerization (EP) require an electrical input to perform the polymerization. EP provides several advantages vs chemical methods as: it is faster, controlable, does not require toxic oxidant and doping can be modulated. The addition of the CNTs within the reaction can produce nucleation processes in the electrode assisting the formation of 3D structures. Therefore, template agents can be added to allow polymerization along the interstices. In our lab, we manufacture large 3D PEDOT/CNT scaffolds using this technique. From the best of our knowledge, we have manufacture by first time real 3D structures thicker than 1mm of height. Besides, the role of CNTs during the polymerization observed by SEM as well as in the impact in the conductivity. SH-SY5Y cells were culture on the scaffolds during 3 and 7 days. The in vitro analyses suggest the differentiation into neuronal cells due to the presence of β-tubulin class III and MAP-II target proteins mainly expresses in neurons.[19] This technique is very modulable thanks to different monomers can be used. In the same manner, we developed different scaffolds of copolymerization with a bi-functional EDOT (bisPEDOT) monomer forming PEDOT-*co*-bisPEDOT scaffolds. Moreover, due to the copolymerization rates, composition, porosity and thickness of the material was modulated. As well, the electrochemical performance changed between the different percentages of the scaffolds.[20]

## 3. Conclusion and future perspectives

The combination of CNTs and conjugated polymers into 3D scaffolds have demonstrated to improve the resulting hybrid behavior in terms of conductivity and mechanophysical properties and, at the same time, produce new properties such as increased thermal characteristics. The synergy of CNT and CP strengthens the nanocomposites, creating new generation of devices with unique capabilities and ease to tune their properties in a reproducible manner.

In our experience, we have overcome the low processability and dispersibility of both materials, CNT and CPs, developing new strategies to obtain a good homogeneity and mixed structures, thus yielding novel and advanced hybrid composites with an excellent symbiosis between the properties provided by each of the conductive materials. Furthermore, they have huge potential for up-scaling

and industrialization in numerous applications.

The brilliant interface between CNT and neuronal networks, together with their inherent conductivity, large surface area and functionalization ability, have placed them as one of the most promising nanomaterials with great potential for engineering of constructs to promote the growth of electroactive tissues. More specifically, the ability of CNTs to change the electrical properties of neurons makes them great candidates for novel tissue engineering of other electroactive cells, in particular, of myocyte cells, that have not yet been fully exploited. In particular, CNT/CP hybrids may yield mainstream technologies that require stretchable, self-healing, wearable and waterproof electronic devices in the near future, for multifunctional supercapacitors with an extremely long lifespan. On the other hand, 3D printing of carbon nanomaterials has not been explored yet, being this one of the pending paths in 3D biomedical technologies. [21]

Overall, the large list of combinations and approaches to fabricate new conductive CNT/CP-containing hybrid materials is increasing exponentially every day. However, above all, the challenge is to find an outstanding combination of one of the CNT with a CP in a determined architecture for each specific combination. The possibilities are almost infinite and, therefore, the game has only just begun.

## 4. References


[1] Loh Q.L, and Choong C, Three-dimensional scaffolds for tissue engineering applications: role of porosity and pore size. Tissue engineering. Part B, Reviews 2013; 19(6), 485–502.

[2] Alegret N, Dominguez-Alfaro A, Mecerreyes D, 3D Scaffolds Based on Conductive Polymers for Biomedical Applications. Biomacromolecules 2019, 20(1), 73-89

[3] Gómez IJ, Vázquez Sulleiro M, Mantione D, Alegret N. Carbon Nanomaterials Embedded in Conductive Polymers: A State of the Art. Polymers (Basel) 2021, 27;13(5):745

[4] De Volder MF, Tawfick SH, Baughman RH, Hart AJ. Carbon nanotubes: present and future commercial applications. Science 2013, 339(6119):535-9

[5] Accardo A, Cirillo C, Lionnet S, Vieu C, Loubinoux I. Interfacing cells with microengineered scaffolds for neural tissue reconstruction. Brain Res Bull 2019, 152:202-211

[6] Ince Yardimci, Atike, Hande Aypek, Ozgur Ozturk, Selahattin Yilmaz, Engin Ozcivici, Gulistan Mese, and Yusuf Selamet. CNT Incorporated Polyacrilonitrile/ Polypyrrole Nanofibers as Keratinocytes Scaffold. Journal of Biomimetics, Biomaterials and Biomedical Engineering 2019, 41: 69–81

[7] Rao, B.S. and Pathak, S.K., Thermal and viscoelastic properties of sequentially polymerized networks composed of benzoxazine, epoxy, and phenalkamine curing agents 2006, J. Appl. Polym. Sci., 100: 3956-3965

[8] Sharma Y, Tiwari A, Hattori S, Terada D, Sharma AK, Ramalingam M, Kobayashi H. Fabrication of conducting electrospun nanofibers scaffold for three-dimensional cells culture. Int J Biol Macromol 2012, 51(4):627-31

[9] Nayagam DA, Williams RA, Chen J, Magee KA, Irwin J, Tan J, Innis P, Leung RT, Finch S, Williams CE, Clark GM, Wallace GG. Biocompatibility of immobilized aligned carbon nanotubes. Small 2011, 18;7(8):1035-42

[10] S. Li, Z. P. Guo, C. Y. Wang, G. G. Wallace, H. K. Liu, Flexible cellulose based polypyrrole–multiwalled carbon nanotube films for bio-compatible zinc batteries activated by simulated body fluids 2013, J. Mater. Chem. A, 1, 14300.

[11] Cai-Wan Chang-Jian, Er-Chieh Cho, Kuen-Chan Lee, Jen-Hsien Huang, Po-Yu Chen, Bo-Cheng Ho, Yu-Sheng Hsiao, Thermally conductive polymeric composites incorporating 3D MWCNT/PEDOT:PSS scaffolds, Composites Part B: Engineering 2018, 136, 46-54

[12] Jayaram Akhila K., Pitsalidis Charalampos, Tan Ellasia, Moysidou Chrysanthi-Maria, De Volder Michael F. L., Kim Ji-Seon, Owens Roisin M., 3D Hybrid Scaffolds Based on PEDOT: PSS/MWCNT Composites, Frontiers in Chemistry 2020, 8, 698

[13] Zexing Deng, Yi Guo, Xin Zhao, Peter X. Ma, and Baolin Guo, Multifunctional Stimuli-Responsive Hydrogels with Self-Healing, High Conductivity, and Rapid Recovery through Host–Guest Interactions 2018, Chemistry of Materials 30 (5), 1729-1742

[14] Shin J, Choi EJ, Cho JH, Cho AN, Jin Y, Yang K, Song C, Cho SW. Three-Dimensional Electroconductive Hyaluronic Acid Hydrogels Incorporated with Carbon Nanotubes and Polypyrrole by Catechol-Mediated Dispersion Enhance Neurogenesis of Human Neural Stem Cells. Biomacromolecules 2017, 9, 18(10):3060-3072

[15] Nodora, K. M. A., Yim, J.-H., Elucidation of the Controversial Layer Growth Mechanism of Vapor Phase Polymerization in the Preparation of Conductive Poly(3,4-ethylenedioxythiophene)-SiO2 Hybrid Films, Adv. Mater. Interfaces 2020, 7, 2000046

[16] Jin Seul Park, Hoe Jin Kang, Byong-Taek Lee, Jong Seob Choi, and Jin-Heong Yim, Mechanically and Electrically Enhanced Polyurethane-poly(3,4-ethylenedioxythiophene) Conductive Foams with Aligned Pore Structures Promote MC3T3-E1 Cell Growth and Proliferation, ACS Applied Polymer Materials 2020, 2 (4), 1482-1490

[17] Alegret N, Dominguez-Alfaro A, González-Domínguez JM, Arnaiz B, Cossío U, Bosi S, Vázquez E, Ramos-Cabrer P, Mecerreyes D, Prato M. Three-Dimensional Conductive Scaffolds as Neural Prostheses Based on Carbon Nanotubes and Polypyrrole. ACS Appl Mater Interfaces 2018, 19, 10(50):43904-43914

[18] Dominguez-Alfaro A, Alegret N, Arnaiz B, et al. Tailored Methodology Based on Vapor Phase Polymerization to Manufacture PEDOT/CNT Scaffolds for Tissue Engineering. ACS Biomaterials Science & Engineering 2020, 6(2):1269-1278

[19] Antonio Dominguez-Alfaro, Nuria Alegret, Blanca Arnaiz, Maitane Salsamendi, David Mecerreyes, and Maurizio Prato, Toward Spontaneous Neuronal Differentiation of SH-SY5Y Cells Using Novel Three-Dimensional Electropolymerized Conductive Scaffolds, ACS Applied Materials & Interfaces 2020, 12 (51), 57330-57342

[20] Dominguez-Alfaro, A.; Gómez, I.J.; Alegret, N.; Mecerreyes, D.; Prato, M. 2D and 3D Immobilization of Carbon Nanomaterials into PEDOT via Electropolymerization of a Functional Bis-EDOT Monomer, Polymers 2021, 13, 436

[21] Miryam Criado-Gonzalez, Antonio Dominguez-Alfaro, Naroa Lopez-Larrea, Nuria Alegret, and David Mecerreyes,

[21] Miryam Criado-Gonzalez, Antonio Dominguez-Alfaro, Naroa Lopez-Larrea, Nuria Alegret, and David Mecerreyes, Additive Manufacturing of Conducting Polymers: Recent Advances, Challenges, and Opportunities, ACS Applied Polymer Materials 2021, 3 (6), 2865-2883

**Dr. Núria Alegret** obtained her BS in Chemistry, MS in Computational Chemistry (2010) and MS in Nanoscience and Nanotechnology (2012) from the University Rovira i Virgili (URV). She obtained her Ph.D. degree in 2014 awarded the Excellence Recognition under the supervision of Prof. Josep M. Poblet (URV). In 2015, Núria joined the group of Prof. Maurizio Prato as a post-doctoral researcher in the Univeristy of Trieste (Italy). In 2016, she was transferred to the second laboratory of Prof. Prato in the CIC BiomaGune center in San Sebastian (Spain), where she is leading the area of design and synthesis of CNT-based 3D scaffolds for nerve and cardiac tissue engineering. In 2018, she was awarded a Global Marie Curie Fellowship and moved to Prof. Luisa Mestroni group at the Cardiology Department (UC Denver), where performed *in vitro* studies and expanded her knowledge and skills in the biomedical application of 3D CNT-based scaffolds for cardiac tissue engineering. In 2020, she moved to Prof. Mecerreyes laboratory (UPV/EHU, Spain) to develop new kind of scaffolds and conductive hydrogels. Currently, she came back to Prof. Prato's laboratory at CIC biomaGUNE where she is expanding the development of 3D conductive scaffolds and hydrogels, evaluating them as electroactive tissue regeneration devices. In addition, she is closely collaborating with Biodonostia HRI in developing *in vitro* studies to test the new scaffolds she is producing, bringing all the knowledge acquired, expanding her knowledge in cardiac muscular dystrophies and establishing the new field of cardionanoscience that she developed in the USA.

# Some insights into the evolution of support surface chemistry during the preparation of metal oxide-activated carbon catalysts by conventional wet impregnation

## Nuevos avances sobre la evolución de la química superficial del soporte durante la preparación de catalizadores óxido metálico-carbón activado mediante impregnación húmeda convencional

**A. Barroso Bogeat*[1], M. F. Alexandre Franco[2], C. Fernández González[2], V. Gómez Serrano[2]**

*[1] Departamento de Química Inorgánica, Facultad de Farmacia, Universidad de Salamanca, C/ Licenciado Méndez Nieto s/n, 37007 Salamanca, España*

*[2] Departamento de Química Orgánica e Inorgánica, Facultad de Ciencias, Universidad de Extremadura, Avda. de Elvas s/n, 06006 Badajoz, España*

**Corresponding author: adrianbogeat@usal.es*

**Abstract**

The present work is aimed at unveiling the evolution and changes undergone by the surface chemistry of a carbon support, with special attention to the oxygen-containing functionalities, during the different steps involved in the preparation of activated carbon (AC)-metal oxide (MO) catalysts by the conventional wet impregnation method. For such an aim, three series of catalyst samples have been prepared by impregnation of a commercial AC (Merck) with $Fe(NO_3)_3$ and $Zn(NO_3)_2$ aqueous solutions at 80 °C for 5 h, followed by oven-drying at 120 °C for 24 h, and then heat treatment at 200 or 850 °C for 2 h under inert atmosphere. Both the raw AC and the resulting samples were characterised in terms of their surface chemistry by FT-IR spectroscopy and measurement of pH of the point of zero charge. Chromene, pyrone, and ether type structures are by far dominant in the AC surface. The hydrolysis of $Fe^{3+}$ and $Zn^{2+}$ cations markedly influences the pH of the impregnation solution and thereby the oxidation of surface functional groups and structures of AC by the nitrate ion present in such solutions. Thus, the degree of oxidation is larger for the $Fe^{3+}$ aqueous solution than for that of $Zn^{2+}$. During the impregnation step, phenolic hydroxyl or carboxylic acid groups as well as C-O-M bonds are usually formed on the AC surface by oxidation of chromene, 2-pyrone, and ether-type structures. Concerning the heat-treated samples, chemical changes are much stronger for the catalysts prepared at 850 °C as compared to those obtained at 200 °C. At the higher temperature, carboxylic acid groups, 4-pyrone, metal carboxylate structures, and C-O-M atomic groupings are formed.

**Resumen**

El presente trabajo tiene como objetivo desvelar la evolución y los cambios experimentados por la química superficial de un soporte carbonoso, con especial atención a las funcionalidades oxigenadas, durante las diferentes etapas implicadas en la preparación de catalizadores carbón activado (AC)-óxido metálico (MO) mediante el método de impregnación húmeda convencional. Para este propósito, tres series de catalizadores se han preparado mediante impregnación de un AC comercial (Merck) con disoluciones acuosas de $Fe(NO_3)_3$ y $Zn(NO_3)_2$ a 80 °C durante 5 h, seguida de secado en estufa a 120 °C durante 24 h y, por último, tratamiento térmico a 200 o 850 °C durante 2 h bajo atmósfera inerte. Tanto el AC de partida como las muestras resultantes fueron caracterizadas en términos de su química superficial mediante espectroscopía FT-IR y medida del pH del punto de carga cero. La superficie del AC está dominada por estructuras tipo cromeno, pirona y éter. La hidrólisis de los cationes $Fe^{3+}$ y $Zn^{2+}$ influye decisivamente sobre el pH de la disolución de impregnación y, en consecuencia, sobre la oxidación de los grupos funcionales y estructuras superficiales del AC por el ion nitrato presente en tales disoluciones. Así, el grado de oxidación es mayor para la disolución acuosa de $Fe^{3+}$ que para la de $Zn^{2+}$. Grupos hidroxilo fenólico y ácido carboxílico, así como enlaces C-O-M, se forman sobre la superficie del AC durante la etapa de impregnación por oxidación de estructuras tipo cromeno, 2-pirona y éter. En cuanto a las muestras tratadas térmicamente, los cambios químicos son mucho más intensos para los catalizadores preparados a 850 °C en comparación con los obtenidos a 200 °C. A la máxima temperatura de tratamiento se forman grupos ácido carboxílico, 4-pirona, estructuras de carboxilatos metálicos y grupos atómicos C-O-M.

### 1. Introduction

Activated carbon (AC, hereafter) is a porous carbon material widely employed not only as adsorbent but also as catalyst and catalyst support [1–3]. Such an extensive use chiefly arises from its unique and excellent properties, among which the high specific surface area, tunable porous structure, and very rich surface chemistry are worth mentioning. Concerning this latter, a number of works have revealed the pivotal role played by the surface chemical features

of AC in catalytic processes due to its broadly varied reactivity, thus governing the dispersion of the catalytic active phase, its loading, and even the catalytic activity and/or selectivity [4–9]. In the field of carbon-based materials, the term "surface chemistry" commonly refers to the chemical nature and properties of their surface, which is essentially made up of unpaired electrons and several heteroatoms [10]. These latter are present in markedly different quantities and bonded to the carbon skeleton, thus forming a variety of surface functional groups and structures identical to those typically described for aromatic organic compounds [10,11]. Among the various heteroatoms found in ACs, oxygen is by far the most abundant and important, followed by nitrogen and to a much lesser extent hydrogen and phosphorus. In fact, carbon-oxygen functional groups not only influence the surface behaviour, wettability, or electrical, adsorptive, and catalytic properties of ACs, but also allow tailoring and tuning the surface chemistry for a given specific application by means of functionalisation [12].

On the other hand, metal oxides (MO, henceforth) are ubiquitous materials in heterogeneous catalysis due to their redox and acid-base properties, which allow them to take part in chemical processes involving the exchange of electrons, protons, and oxide ions. Therefore, a combination of AC and MO properties in a single hybrid catalyst may render it more versatile in catalysis processes and this redounds the number of applications.

The present work is aimed at preparing a series of AC-MO catalysts by conventional wet impregnation of a commercial AC support with $Fe(NO_3)_3$ and $Zn(NO_3)_2$ aqueous solutions under mild conditions and subsequent heat treatment of the resulting products at higher temperatures. Then, the as-prepared catalysts are characterised by means of FT-IR spectroscopy and measurement of the point of zero charge with a view to shedding light on the evolution and changes undergone by the surface chemistry of the carbon support, with special attention to the oxygen functional groups and structures, during the set of steps involved in the preparation of the samples (i.e., soaking, oven-drying, and calcination). The results obtained in previous characterisation studies of both AC and the freshly prepared AC-MO catalysts have been previously reported elsewhere [13–18].

## 2. Experimental

### *2.1. Materials and reagents*

As received without any additional treatment, a commercial granular AC purchased from Merck (Darmstadt, Germany), 1.5 mm average grain size, was employed as support. This carbon material had been previously characterised by our research group in terms of its elemental chemical composition, surface chemistry, and textural features, the results being reported elsewhere [13,14,17]an attempt is made here to identify not only pyrone and chromene type structures but also their isomers in a commercial activated carbon (Merck; AC. Briefly, AC possesses a much lower ash content (i.e., around 4.7 wt.%) as compared to other activated carbons, and it is an essentially microporous material (micropore volume, 0.36 $cm^3 \cdot g^{-1}$; apparent surface area, 711 $m^2 \cdot g^{-1}$) with a noticeable contribution both of meso- and macroporosity (mesopore volume, 0.15 $cm^3 \cdot g^{-1}$; macropore volume, 0.21 $cm^3 \cdot g^{-1}$).

Metal nitrates (i.e., $Fe(NO_3)_3 \cdot 9H_2O$ and $Zn(NO_3)_2 \cdot 6H_2O$), which are as a rule readily soluble in water, were selected as metal oxide precursors and supplied by Panreac (Barcelona, Spain; reagent grade).

### *2.2. Preparation of the AC-MO catalysts*

Metal oxide phases were supported on the pristine AC material by using a conventional wet impregnation method in two successive stages, according to the procedure previously described in detail elsewhere [14,16]activated carbon (AC. Briefly, AC was soaked at 80 °C for 5 h in an aqueous solution prepared by dissolving the appropriate amount of the metal nitrate precursor (i.e., precursor to AC mass ratio of 1:1). Then, the resulting impregnated solids were oven-dried at 120 °C for 24 h and finally heat-treated at either 200 or 850 °C for 2 h under dynamic inert atmosphere. Overall, three series of AC-MO catalysts were obtained depending on the heating temperature (i.e., 120, 200, and 850 °C) and therefore three samples for each employed metal precursor (i.e., $Fe(NO_3)_3 \cdot 9H_2O$ and $Zn(NO_3)_2 \cdot 6H_2O$). These samples have been denoted as MT, with M standing for the initial letter of the symbol for the metal and T for the heat treatment temperature.

### *2.3. Characterisation of the AC-MO catalysts*

The as-prepared AC-MO catalyst samples were characterised in terms of their surface chemical features by means of FT-IR spectroscopy and measurements of the pH of the point of zero charge. These jointly provided a detailed picture of the evolution and changes undergone by the surface chemistry of the carbon support as a result of the soaking, oven-drying, and heating steps involved in the preparation of the supported catalysts.

#### *2.3.1. Fourier-FT-IR spectroscopy*

FT-IR spectra were registered for both the raw AC support and the freshly prepared catalyst samples by using a PerkinElmer Spectrum 100 spectrophotometer, in the wavenumber range from 4000 to 400 $cm^{-1}$ and averaging the data from 8 successive scans taken at 2 $cm^{-1}$ resolution. Prior to acquiring these spectra, sample/KBr pellets with a total mass of 238 mg and a sample to KBr mass ratio of 1:1900 were prepared following the procedure described in detail elsewhere [13]an attempt is made here to identify not only pyrone and chromene type structures but also their isomers in a commercial

activated carbon (Merck; AC. The spectrum for a pure KBr pellet with approximately the same mass as the sample pellets was recorded and employed as background.

*2.3.2. pH of the point of zero charge ($pH_{pzc}$)*

The $pH_{pzc}$ for both the AC and the supported catalysts was measured by using the procedure proposed by Newcombe et al [19]. In brief, a set of 0.01 mol·$L^{-1}$ NaCl aqueous solutions at pH of around 2, 4, 6, 8, and 10 were prepared by adjusting these values with either 0.1 mol·$L^{-1}$ HCl or NaOH aqueous solutions. Then, the $pH_{pzc}$ for each sample was determined from the plot of pH of the initial solution against pH of the corresponding supernatant after a soaking time of 48 h.

## 3. Results and discussion

### *3.1. Infrared analysis*

The results obtained in the study of the pristine AC employed as support by means of FT-IR spectroscopy have been previously discussed elsewhere [13]an attempt is made here to identify not only pyrone and chromene type structures but also their isomers in a commercial activated carbon (Merck; AC, so they are herein summarised only for the sake of comparison. The infrared spectrum recorded for the AC is depicted in Figure 1, while the main band assignments and positions are summarised in Table 1. The most prominent feature of this spectrum is the very strong band centred at around 1720 $cm^{-1}$, which is ascribed to the *ν*(C=O) vibration of both carboxylic acid groups and 2-pyrone structures, which are involved in hydrogen bonding. Moreover, the presence of carboxylic acid groups in the carbon support is further evidenced by the couple of bands registered at 1279 and 901 $cm^{-1}$. On the other hand, a large number of spectral features, such as the bands and shoulders at 1657, 1636, 1249, 1024, 740, and so on, $cm^{-1}$, are tentatively attributed to chromene and/or pyrone type structures (which are henceforth referred to as CPS in the text). Furthermore, the band appearing at about 1024 cm-1 is associated with ether type structures. Finally, the total content of phenolic hydroxyl groups (C-OH) in the AC surface is expected to be low, according to the small absorption of infrared radiation observed at around 1200 $cm^{-1}$.

The infrared spectra registered for the three catalyst samples of *FT* series are plotted together in Figure 2 for comparison purposes. As compared to that obtained for the raw AC (see Figure 1), the spectrum of F120 displays two stronger and well-defined bands located at 1726 and 1283 $cm^{-1}$, whereas the band at 1021 $cm^{-1}$ is markedly weaker. Accordingly, it is likely that during the impregnation of the AC support with the $Fe^{3+}$ aqueous solution (starting pH 1.54) CPS are oxidised as well and transformed into carboxylic acid groups. In addition, infrared absorption decreases in the range from 1236 to 1165 $cm^{-1}$ while the band at 1112 $cm^{-1}$ is significantly broader and stronger, all these spectral changes being consistent with the presence of C-O-Fe atomic groupings. These latter are formed by C-OH and Fe-OH condensation reactions accompanied by water release. Also, $O_2$ chemisorbed in the F120 sample may absorb infrared radiation nearby 1112 $cm^{-1}$. Furthermore, the scarcely visible shoulder at around 1386 $cm^{-1}$ reveals that the content of residual nitrate groups ($NO_3^-$) is rather low in F120.

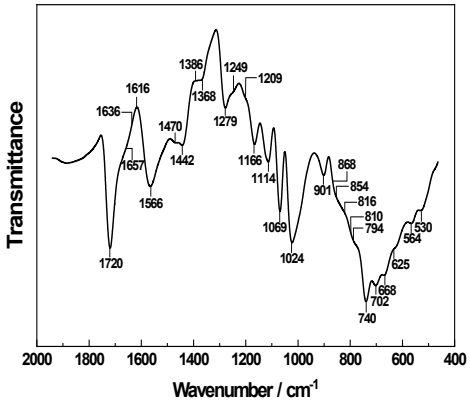


**Figure 1.** FT-IR spectrum registered for the raw AC support.

**Figura 1.** Espectro FT-IR registrado para el soporte AC.

**Table 1.** FT-IR spectrum of the AC support. Main band assignments.

**Tabla 1.** Espectro FT-IR del soporte AC. Asignaciones de bandas principales.

| Spectral feature | Position / $cm^{-1}$ | Assignment[a] | Functional group / structure |
|---|---|---|---|
| Peaks | 2972-2823 | ν(C-H) | Chromene structures |
| | | ν(O-H) | Quinone oximes |
| Band | 1720 | ν(C=O) | Carboxylic acid group, 2-pyrone structures |
| Shoulder | 1657 | ν(C=O) | Pyrone and chromene structures, carbonyl structures |
| Shoulder | 1636 | ν(C=C) | Pyrone and chromene structures |
| Band | 1566 | $\nu_s$(C=C) skeletal | Aromatic ring |
| | | ν(C=C) | 2-pyrone structures |
| Band | 1279 | δ(O-H)-ν(C-O) | Carboxylic acid |
| | | $\nu_{as}$(=C-O-C) | 4H-chromene |
| Shoulders | ca. 1249 | $\nu_{as}$(=C-O-C) | 2H-chromene, 2-pyrone |
| Band | 1024 | $\nu_s$(=C-O-C) | Chromene, pyrone, ether structures |

[a]Abbreviations: ν, stretching; δ, bending (in-plane); as, asymmetric; s, symmetric.

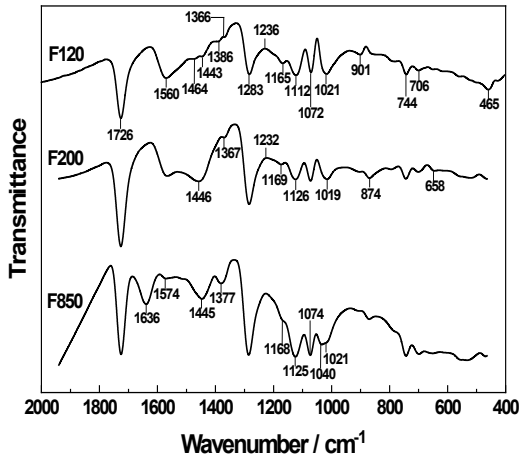


**Figure 2.** FT-IR spectra registered for the catalyst samples of *FT* series.

**Figura 2.** Espectros FT-IR registrados para las muestras de catalizador de la serie *FT*.

The greater intensity of the bands at 1726 and 1283 $cm^{-1}$ for F200 than for F120 suggests that the heat treatment of this latter sample at 200 °C for 2 h under inert atmosphere promotes the formation of carboxylic acid groups to some extent. Similarly to the preparation of F120, these groups are likely generated from CPS since their total content is lower for the F200 catalyst sample than for F120, as revealed by the noticeably decreased intensity of the band at 1019 $cm^{-1}$ observed in the F200 infrared spectrum. In this latter, infrared radiation absorption clearly decreases between 1232 and 1169 $cm^{-1}$, so phenolic -OH groups may also be involved in the oxidation processes. In this case, the oxidising agent should be any chemical species remaining up-taken after the preparation of F120, as the heat treatment of this sample at 200 °C in the preparation of the F200 catalyst is accomplished in nitrogen atmosphere.

As most prominent modifications, the spectrum recorded for the F850 catalyst sample displays a couple of medium intensity bands at 1636 and 1445 $cm^{-1}$, together with the weaker band centred at 1377 $cm^{-1}$. Moreover, this spectrum exhibits the band at 1125 $cm^{-1}$ with increased intensity in comparison to that peaked at 1040 and 1021 $cm^{-1}$. In the case of the F850 catalyst, carboxylic acid groups, 4-pyrone structures as well as metal carboxylates could be formed due to the heating of F120 sample at 850 °C in inert atmosphere. Nevertheless, this heat treatment seems to favour the formation of C-O-M atomic groupings rather than of M-O-M atomic groupings. In this regard, the former groups may be generated with involvement of carboxylic acid groups, as for metal carboxylates with unidentate coordination [20], rather than of phenolic -C-OH groups, in view that the absorption increases nearby 1200 $cm^{-1}$ for F850. In accordance with these results, it is likely that the main factor controlling the changes produced in the surface chemical composition of the catalyst samples is the reactivity of the metal oxide at high temperature.

The FT-IR spectra recorded for the catalyst samples of the *ZT* series are gathered in Figure 3. As far as the spectrum for Z120 is concerned, it displays three shoulders at around 1657, 1636, and 743 $cm^{-1}$. Moreover, the strong band located at 1024 cm-1 for the raw AC support is absence in the spectrum for Z120, likely because of overlapping bands. However, the increase in the absorption of infrared radiation observed between 1226 and 1161 $cm^{-1}$ is indicative of the formation of phenolic C-OH groups from CPS as a result of the oxidation process. Such assumption is supported by the noticeable shift to lower frequencies and intensity decrease for the band appearing at 1714 $cm^{-1}$ in the Z120 spectrum (i.e., for the carbon support it is centred at around 1720 $cm^{-1}$). Phenolic C-OH groups may also transform into C-O-Zn atomic groupings, as suggested by the development of the strong band at 1048 $cm^{-1}$. In this connection, it is also worth highlighting that the degree of hydrolysis is smaller for the $Zn^{2+}$ cation as compared to $Fe^{3+}$ cation, which should render the condensation reaction of C-OH and M-OH less likely. On the other hand, the band centred at 1048 $cm^{-1}$ is also ascribable to $O_2$ chemisorbed on the Z120 surface. In any event, from the FT-IR spectrum registered for the Z120 sample it becomes evident that the effect of the impregnation of the AC with the $Zn^{2+}$ precursor solution on the surface chemistry of the carbon support is less relevant than when a $Fe^{3+}$ aqueous solution is employed. The much stronger band located at 1384 cm-1 for the Z120 spectrum than for its F120 counterpart reveals that the content of residual nitrate groups is much higher in the former catalyst sample.

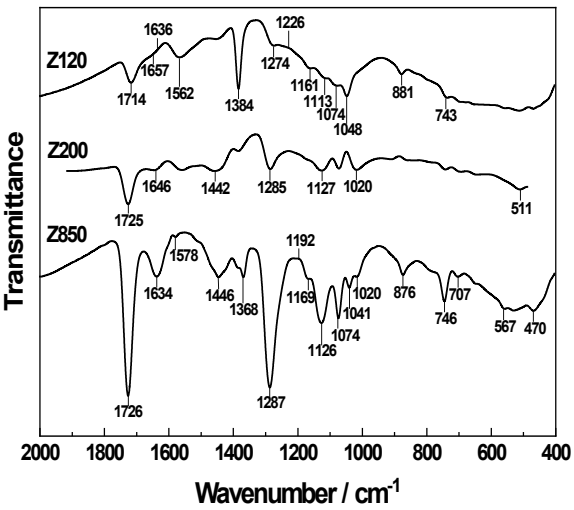


**Figure 3.** FT-IR spectra registered for the catalyst samples of *ZT* series.

**Figura 3.** Espectros FT-IR registrados para las muestras de catalizador de la serie *ZT*.

From the comparison of the FT-IR spectra registered for the Z120 and Z200 catalysts, it follows that the heat treatment of the former at 200 °C for 2 h in inert atmosphere leads to an increased concentration of carboxylic acid groups in the surface of the resulting Z200 catalyst sample. Regarding the spectrum for Z850, the presence of a large number of well-defined bands centred at 1726, 1634, 1446, 1368, 1126, 1074, 1041, 876, and 746 $cm^{-1}$ is worth mentioning.

In addition, an absorption decrease is also noted for the band peaked at 1020 $cm^{-1}$. Accordingly, it becomes apparent that the heat treatment of the oven-dried Z120 sample at 850 °C brings about a significant development of oxygen-containing surface groups. To sum up, from the FT-IR spectra recorded for the couple of catalyst samples prepared by heat treatment at 850 °C (i.e., F850 and Z850) it is concluded that their surface chemistries are rather similar. Furthermore, according to the relative band intensities, the concentration of surface functional groups and structures or atomic groupings for these latter catalysts varies in the following order: Z850 > F850, carboxylic acid; F850 ≈ Z850, 4-pyrone; F850 ≈ Z850, C-O-M.

### *3.2. $pH_{pzc}$*

The $pH_{pzc}$ is 10.50 for the raw AC support [14]activated carbon (AC. As can be seen from Table 2, for the as-prepared AC-MO catalysts it is markedly lower than for the carbon substrate, irrespective of the metal oxide precursor and the heat treatment temperature. This observation is fully consistent with the increase in the content of acidic surface groups and decrease in the content of basic surface structures, as previously inferred from the corresponding FT-IR spectra. Furthermore, it is also found that the $pH_{pzc}$ depends on the metal oxide precursor and the heat treatment temperature. Thus, samples prepared by impregnation with the $Fe^{3+}$ aqueous solution exhibit $pH_{pzc}$ values slightly lower than those observed for their counterparts obtained by impregnation with the $Zn^{2+}$ aqueous solution. Such variation appears to be compatible with a greater presence of carboxylic acid groups in samples of *FT* series and of phenolic hydroxyl groups in those catalysts of *ZT* series. Concerning the influence of the heat treatment temperature, as compared to the samples oven-dried at 120 °C $pH_{pzc}$ first slightly increases for catalysts prepared by heat treatment at 200 °C and then much more sharply for those obtained by heating at 850 °C, thus becoming close to the value measured for the AC support. Finally, it should be noted that although basic structures present in these latter samples must contribute to their basic character, band intensities associated with CPS do not directly correlate with $pH_{pzc}$ values. Therefore, it is expected that other factors, such as the concentration of carboxylic acid groups and whether these functionalities are found as carboxylates or not, must also influence the surface basicity of the catalysts.

**Table 2.** $pH_{pzc}$ values measured for the raw AC support and the as-prepared AC-MO catalyst samples.

**Tabla 2.** Valores de $pH_{pzc}$ medidos para el soporte AC y las muestras de catalizador AC-MO preparadas

| Sample | $pH_{pzc}$ | Sample | $pH_{pzc}$ | Sample | $pH_{pzc}$ |
|---|---|---|---|---|---|
| AC | 10.50 | | | | |
| F120 | 4.00 | F200 | 4.10 | F850 | 8.80 |
| Z120 | 6.30 | Z200 | 6.50 | Z850 | 9.80 |

## 4. Conclusions

The preparation of three series of AC-MO catalyst samples has been carried out by means of the conventional wet impregnation method, consisting in three stages: (i) soaking of a commercial AC support with $Fe(NO_3)_3$ and $Zn(NO_3)_2$ aqueous solutions at 80 °C for 5 h, (ii) oven-drying at 120 °C for 24 h, and (iii) heat treatment at 200 or 850 °C for 2 h under inert atmosphere. The characterisation of the surface chemistry of the as-prepared materials by the FT-IR spectroscopy technique allows to draw the following main conclusions:

1. The impregnation of AC leads to the formation of phenolic hydroxyl and/or carboxylic acid groups as well as of C-O-M bonds to the detriment of CPS and ether type structures found in the raw carbon support. Accordingly, AC impregnation results in a marked increase of the acidic character of the carbon surface, as confirmed from $pH_{pzc}$ measurements. C-O-M atomic groupings are formed by condensation of AC-OH groups and M-OH groups with water release.
2. The heat treatment of the oven-dried samples at 200 or 850 °C brings about stronger chemical modifications when heating at the highest temperature. For these catalysts, in general, carboxylic acid groups, 4-pyrone groups, metal carboxylates, and C-O-M atomic groupings are formed.
3. The chemical changes undergone by the AC surface as a result of its impregnation with the MO precursor solutions and subsequent oven-drying are essentially attributed to the oxidising action of chemical species present in these solutions, such as the nitrate ion, or generated during the soaking treatment. When heating at 200 or 850 °C, the chemical changes are mainly connected with the presence in the samples surface of chemisorbed $O_2$ and thermal effects at high temperature.

## References

[1] Rodríguez-Reinoso F. The role of carbon materials in heterogeneous catalysis. Carbon 1998; 36:159–175.

[2] Rodríguez-Reinoso F, Sepúlveda-Escribano A. Carbon as catalyst support. In: Philippe Serp and José Luis Figueiredo Eds. Carbon materials for catalysis. John Wiley & Sons. 2009 p. 131–155.

[3] Barroso-Bogeat A, Fernández-González C, Alexandre-Franco M, Gómez-Serrano V. Activated carbon as a metal oxide support: A review. In: James F. Kwiatkowski Ed. Activated carbon: classifications, properties and applications. Nova Science Publishers. 2012 p. 297–318.

[4] Calafat A, Laine J, López-Agudo A, Palacios JM. Effect of surface oxidation of the support on the thiophene hydrodesulfurization activity of Mo, Ni, and NiMo catalysts supported on activated carbon. J. Catal. 1996; 162:20–30.

[5] Fraga MA, Mendes MJ, Jordão E. Examination of the surface chemistry of activated carbon on enantioselective hydrogenation of methyl pyruvate over Pt/C catalysts. J. Mol. Catal. A Chem. 2002; 179:243–251.

[6] Huang H-H, Lu M-C, Chen J-N, Lee C-T. Catalytic decomposition of hydrogen peroxide and 4-chlorophenol in the presence of modified activated carbons. Chemosphere 2003; 51:935–943.

[7] Moreno-Castilla C, Pérez-Cadenas AF, Maldonado-Hódar FJ, Carrasco-Marín F, Fierro JLG. Influence of carbon-oxygen surface complexes on the surface acidity of tungsten oxide catalysts supported on activated carbons. Carbon 2003; 41:1157–1167.

[8] Aguilar C, García R, Soto-Garrido G, Arriagada R. Catalytic wet air oxidation of aqueous ammonia with activated carbon. Appl. Catal. B Environ. 2003; 46:229–237.

[9] Bandosz TJ. Surface chemistry of carbon materials. In: Philippe Serp and José Luis Figueiredo Eds. Carbon materials for catalysis. John Wiley & Sons. 2009 p. 45–92.

[10] Barroso-Bogeat A, Alexandre-Franco M, Fernández-González C, Gómez-Serrano V. Activated carbon surface chemistry: Changes upon impregnation with Al(III), Fe(III) and Zn(II)-metal oxide catalyst precursors from NO3− aqueous solutions. Arab. J. Chem. 2019; 12:3963–3976.

[11] Jankowska H, Świątkowski A, Choma J. Active carbon. Ellis Horwood. 1991.

[12] Bandosz TJ, Ania CO. Surface chemistry of activated carbons and its characterization. In: Bandosz TJ Ed. Activated carbon surfaces in environmental remediation. Academic Press. 2006: p. 159–229.

[13] Barroso-Bogeat A, Alexandre-Franco M, Fernández-González C, Gómez-Serrano V. FT-IR analysis of pyrone and chromene structures in activated carbon. Energy and Fuels 2014; 28:4096–4103.

[14] Barroso-Bogeat A, Alexandre-Franco M, Fernández-González C, Gómez-Serrano V. Preparation of activated carbon-metal oxide hybrid catalysts: textural characterization. Fuel Process. Technol. 2014; 126:95–103.

[15] Barroso-Bogeat A, Alexandre-Franco M, Fernández-González C, Sánchez-González J, Gómez-Serrano V. Electrical conductivity of metal (hydr)oxide–activated carbon composites under compression. A comparison study. Mater. Chem. Phys. 2015; 152:113–122.

[16] Barroso-Bogeat A, Alexandre-Franco M, Fernández-González C, Gómez-Serrano V. Preparation and microstructural characterization of activated carbon-metal oxide hybrid catalysts: New insights into reaction paths. J. Mater. Sci. Technol. 2015; 31: 806–814.

[17] Barroso-Bogeat A, Alexandre-Franco M, Fernández-González C, Gómez-Serrano V. Preparation of activated carbon-metal (hydr)oxide materials by thermal methods. Thermogravimetric-mass spectrometric (TG-MS) analysis. J. Anal. Appl. Pyrolysis. 2015; 116: 243–252.

[18] Barroso-Bogeat A, Alexandre-Franco M, Fernández-González C, Gómez-Serrano V. Physico-chemical characterization of activated carbon–metal oxide photocatalysts by immersion calorimetry in benzene and water. J. Therm. Anal. Calorim. 2016; 125:65-74.

[19] Newcombe G, Hayes R, Drikas M. Granular activated carbon: importance of surface properties in the adsorption of naturally occurring organics. Colloids Surfaces A Physicochem. Eng. Asp. 1993; 78:65–71.

[20] Palacios EG, Juárez-López G, Monhemius AJ. Infrared spectroscopy of metal carboxylates: II. Analysis of Fe(III), Ni and Zn carboxylate solutions. Hydrometallurgy. 2004; 72:139–148.

**Adrián Barroso Bogeat** (Villafranca de los Barros, Badajoz, October 19th 1987) obtained his Bachelor's degree in Chemistry from the University of Extremadura (UEx, Spain) in 2010. He started his research career as a predoctoral fellow in the "Carbon Adsorbents-Adsorption" (ACA) group, leaded by Professor Vicente Gómez Serrano, at the Department of Organic and Inorganic Chemistry of UEx, supported first by a FPI fellowship from Junta de Extremadura (January 2011 to July 2012) and subsequently by a FPU fellowship from the Spanish Ministry of Education (July 2012 to January 2015). Adrián achieved his PhD in Chemical Science and Technology from UEx in December 2015, being awarded with the Extraordinary Doctorate Award and the 2016 Research Prize by the Spanish Royal Academy of Doctors. In February 2015, he joined the "Solid State Chemistry and Catalysis" group at the Department of Materials Science and Metallurgical Engineering and Inorganic Chemistry of the University of Cádiz (UCA). In this group, he occupied different positions: Research Assistant (February 2015 to August 2017), "Juan de la Cierva-Formación" Postdoctoral Fellow (September 2017 to August 2019), and Postdoctoral Research Associate (September 2019 to April 2021). Very recently, he obtained an Assistant Professor position at the Department of Inorganic Chemistry of the University of Salamanca (USAL).

His current research interests mainly focus on the field of heterogeneous catalysis, particularly the synthesis and physico-chemical characterisation of novel nanostructured catalysts based on rare earth oxides and first-row transition metals, as well as their testing in environmental protection related processes. Dr. Barroso Bogeat has also developed an intense research activity in the field of carbon materials and metal oxide-carbon hybrid materials, with a view

to their applications in environmental protection, heterogeneous catalysis, and energy storage. In this regard, it is also worth highlighting his extensive experience in the study of the electrical properties of carbon materials, metal oxides, and carbon-based hybrid materials.

He has complemented his scientific formation with a three-month predoctoral stay at the Institute of Carbon Science and Technology (INCAR-CSIC, Oviedo, Spain) and a five-month postdoctoral stay at the Department of Chemistry of the University of Copenhagen (Denmark), this latter funded by the "José Castillejo Programme" of the Spanish Ministry of Education. During these stays, he was trained on the electrochemical characterisation of different carbon materials, as well as on electrocatalytic tests in solution by using electrodes based on rare earth oxides.

Finally, Dr. Barroso Bogeat has been a reviewer for several high impact journals in the fields of Materials Science and Chemistry and served as guest editor of a special issue of the *Catalysts* journal devoted to compiling some of the new research trends in rare earth oxide-based catalysts. He has also been member of the Organising Committee of the "XI Meeting of the Spanish Carbon Group" (Badajoz, Spain, October 2011) and Chairman of the Organising Committee of the "XIV Young Researchers Symposium of the Spanish Royal Society of Chemistry (RSEQ)" (Badajoz, Spain, November 2017). Since November 2018, he is president-elect of the Territorial Section of Extremadura (STExt) of the RSEQ.

# Can we systematically screen millions of chemical structures for cost-effective carbon capture?

## ¿Podemos cribar sistemáticamente millones de estructuras químicas para una captura de carbono económica?

**Charithea Charalambous[1], Fergus Mcilwaine[1], Elias Moubarak[2], Berend Smit[2], Susana Garcia[1]***

*[1] Research Centre for Carbon Solutions (RCCS), School of Engineering and Physical Sciences, Heriot-Watt University, EH14 4AS, Edinburgh, UK.*

*[2] Laboratory of Molecular Simulation (LSMO), Institut des Sciences et Ingénierie Chimiques, Ecole Polytechnique Fédérale de Lausanne (EPFL), Rue de l'Industrie 17, CH-1951 Sion, Switzerland.*

** s.garcia@hw.ac.uk*

**Abstract**

Finding the optimal solid adsorbent to capture $CO_2$ for a given source of $CO_2$ and sink (destination) of $CO_2$ is an interesting scientific and technological question. There are millions of materials to choose from and we lack the capacity to synthesize and test all of them. In this work, we show how one can computationally screen thousands of materials and identify the best performing ones by using process-driven key performance indicators that are representative of a capture process that is specifically design for a particular $CO_2$ source and sink. As an illustration of the methodology, we use as an example the capture of $CO_2$ from a waste-to-energy power plant.

### Introduction

There is an urgent global effort to harness the momentum of the Paris Agreement and to limit global warming to well below 2 ºC compared to pre-industrial levels. To achieve this, many countries have made commitments to reach net-zero by mid-century. The sense of urgency is apparent: financial and political climate-related investment has dramatically increased, emission mitigation technology is being deployed at an accelerated rate, and researchers focus on finding economically viable solutions to meet the Paris climate targets.

The vast majority of greenhouse gas emissions ($CO_2$ emissions) can be minimised by either reusing the emitted $CO_2$, or preventing the $CO_2$ from being released into the atmosphere through carbon capture and storage. To do so, cost-effective Carbon Capture Utilization and Storage (CCUS) processes are required to be rapidly deployed across a range of different sources of $CO_2$. The existence of many different $CO_2$ sources, $CO_2$ sinks, and economic conditions across the globe requires CCUS technologies to be evaluated on a case by case basis.

Sorbent-based carbon capture is one of the available technologies suitable for the efficient removal of gas impurities aiming to achieve extremely high purities [1]. The two main reasons for this are: (a) the availability of a large spectrum of microporous adsorbents with varying pore structures and surface properties, and (b) the possibility of designing many different process schemes by tailoring generic adsorption separation methods. Materials like metal-organic frameworks (MOFs) are good candidates, as their chemical composition and pore shape can be optimally tuned for particular applications. The challenge here is to effectively screen the large number of available MOFs for their suitability in a carbon capture process.

Usually, a new material is developed with a particular application in mind. There is no indication whether this material could be a good candidate for other applications, unless one could evaluate its performance for every application. With the tools available today, this task is unrealistic. The development of open-access material databases (e.g., CSD, AtomWork, ChemSpider) provides us with the opportunity of efficient data storage, management, query, presentation, and manipulation. Given the wide spread of material development and data storage, there is a recent trend of linking materials to chemical processes for designing cost-effective optimal separation processes. By accessing these large pools of chemical structures and computing their properties, one can evaluate their performance in a particular application. However, these calculations can be very computationally expensive to perform.

Machine learning has been successfully applied to this domain in multiple ways. In certain situations, expensive molecular simulations can be replaced by multipurpose multilayer perceptron (MLP) [2] to predict isotherms. From a process perspective, surrogate models can be developed that mimic detailed carbon capture processes models, requiring only a fraction of the time to compute results [3]. In contrast to screening studies, inverse design can leverage machine learning to generate MOFs with specific properties [4].

Surrogate models require training in order to predict the outcomes of a carbon capture process. A simple case would be to train a surrogate model on a material database to predict key performance indicators (KPIs) for each material. However, selecting the set of materials to train the model is non-trivial. Since only few materials are top performers in many databases, a model trained on such a database is predominantly trained on the poorly performing materials, leading to poor predictions on high performing materials. A more suited approach is to train a model based on a set of materials that give good performance

predictions. This can be done using active learning, where a more detailed process model is queried for interesting materials, the training data is updated, and the surrogate model retrained [5].

The ultimate goal of most screening studies is to determine the top performing materials. In our case, we determine the performance of a material by its KPIs and so it is difficult to identify a top performer without stating which KPI we find more important than others. Instead, we find the Pareto optimal materials, i.e. those set of materials for which no KPI can be improved without loss in another KPI.

Our previous work involved the development of a molecular simulation tool which allowed us to screen thousands of materials for adsorption using their physicochemical and adsorptive properties [6]. Most recently, we extended this work by coupling the molecular simulation tool with process modelling to rank materials for gas separations and for a given set of process metrics, including the overall energy efficiency and process productivity [7]. A 4-step temperature-vacuum swing adsorption (TVSA) process was developed, and its performance was evaluated using an equilibrium-based shortcut model similar, but extended, to that described by Joss et al. [8]. Our TVSA process model is then coupled with molecular simulations in a high-throughput screening platform. The screening platform allows us to evaluate both the physicochemical and adsorptive properties of thousands of microporous structures, including around 300,000 MOFs [6], and their performance for a particular carbon capture application. A simple representation of the screening platform, excluding some of its current features (discussed by Riboldi et al. [7]) for the purpose of this article, is provided in Figure 1.

We compare this approach to one using active learning. We are able to find the same top performers in only a fraction of the time compared to a brute-force technique (i.e., coupling molecular simulations with process modelling to calculate the KPIs of each material). Our strategy uses an adapted version of the $\varepsilon$-PAL method [9], available as a python package named PyePAL [5].

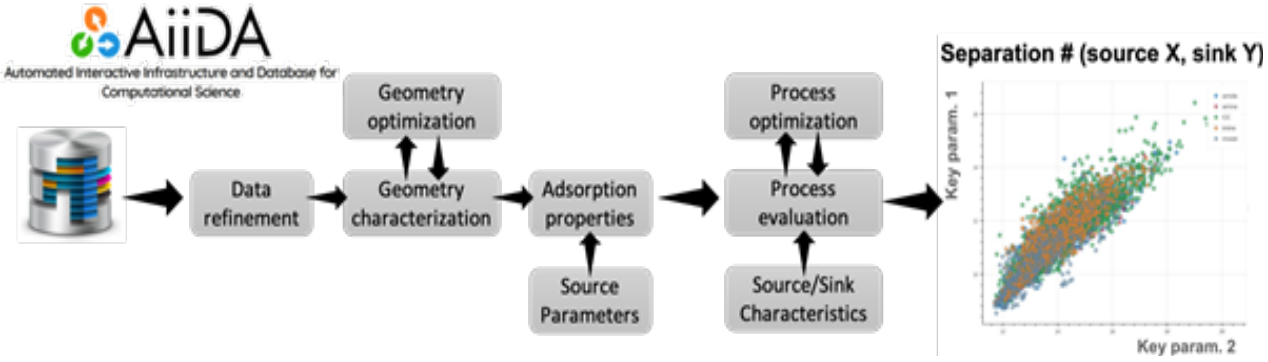


**Figure 1.**The screening platform: The workflow from importing a selected structure from an open-source database to screening and ranking its performance for a particular carbon capture application.

In the following section we provide an example of how the screening platform works for the particular case study of $CO_2$ capture from waste-to-energy power plants. The characteristics of such a flue gas stream are, among others, a $CO_2$ concentration of 13.6 % at 160 ºC temperature and 1 bar pressure. We also compare this to an active learning approach using PyePAL.

### Case Study: Waste-to-Energy

In this article, we applied our TVSA process model to a particular binary mixture of $CO_2$ and $N_2$ ($CO_2$ concentration of 13.6 vol%) for $CO_2$ capture from waste-to-energy power plants. We selected 613 structures for screening and ranked their performance for a specific set of key performance indicators (e.g., specific work used for operating the separation process, $CO_2$ purity of the product stream, and working capacity). The TVSA process is illustrated in Figure 2 and consists of 4 steps: (i) adsorption, (ii) vacuum, (iii) heating under vacuum, and (iv) open cooling (and column pressurization).

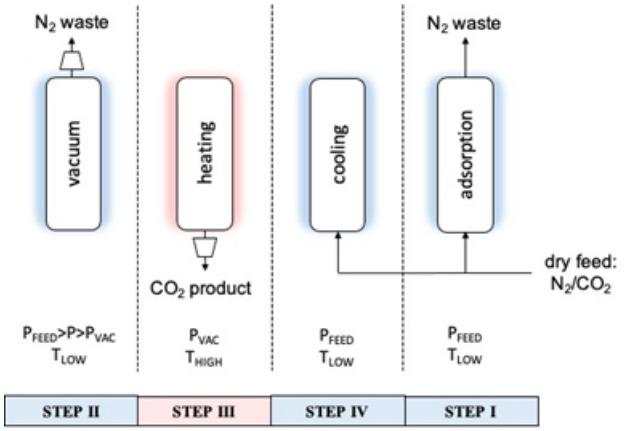


**Figure 2.** A 4-step TVSA process: (i) adsorption, (ii) vacuum, (iii) heating under vacuum, and (iv) open cooling.

Materials can be evaluated in our TVSA process model. For this evaluation the following assumptions were made:

- The feed stream downstream of the adsorption process is available at 20 ºC and 1 bar pressure.
- The temperature at steps (i), (ii), and (iv) is constant at 20 ºC. The temperature at step (iii) is constant at 120 ºC.
- Vacuum at steps (ii) and (iii) is applied at 0.05 bar. The rest of the steps operate at 1 bar pressure.
- The fluid phase is treated as an ideal gas.
- The multi-component adsorption equilibrium is described by the ideal adsorbed solution theory [10] and evaluated using the open-access python package pyIAST [11].
- A heat exchange fluid is used for heating and cooling and its temperature is homogeneous along the column.

As illustrated in the Figure 3, only a small number of the structures perform well for carbon capture from a waste-to-energy power plant.

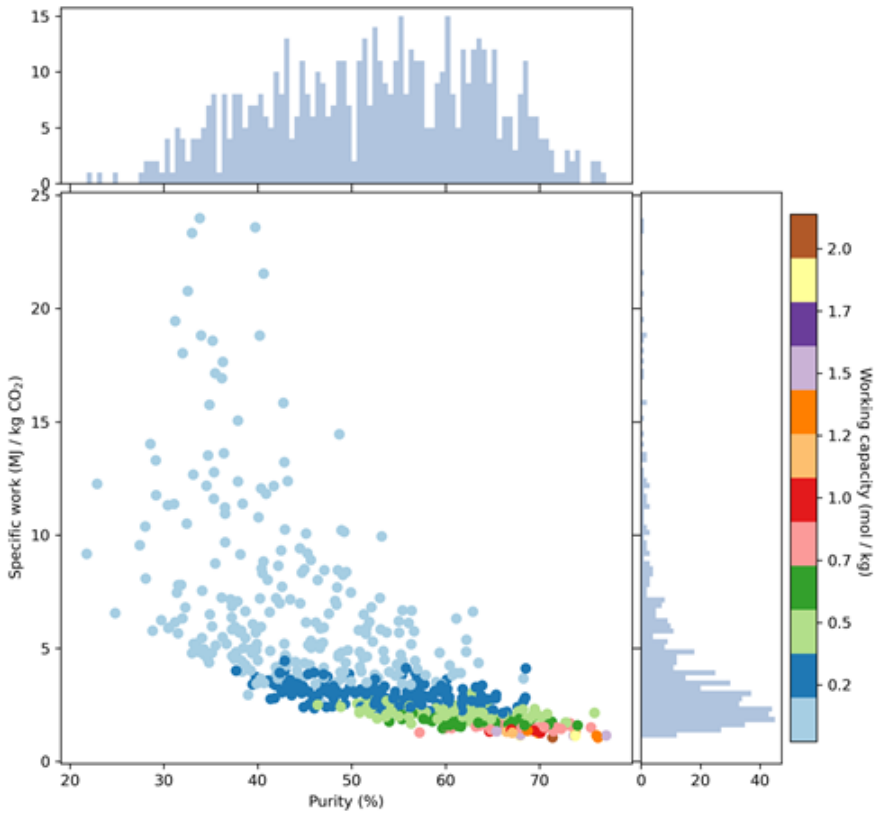


**Figure 3.** Specific work versus $CO_2$ purity and working capacity results from evaluating the performance of 613 structures in the TVSA process for $CO_2$ capture from waste-to-energy power plants. Histograms are shown for each axis.

Screening millions of *in silico* structures is computationally expensive. Evaluating the performance of each of the 613 structures in the TVSA process model took 3 hours (using a 2.7 GHz Dual-Core Intel Core i5 processor). An even more computationally expensive task is computing the physico-chemical (i.e., crystal density, crystal void fraction, heat capacity of the solid) and adsorptive properties (i.e., $CO_2$ and $N_2$ adsorption isotherms and heat of adsorption at different uptakes) of each material. Computing these properties for the 613 structures, which are used as inputs to the TVSA process model, took from 3 to 4 weeks (using an Intel Broadwell based cluster, Fidis [12]).

For the active learning approach, the design space is first initialized by a diverse set of materials. Material descriptors were taken from Seyed et al. [13] and the CoRE-MOF database [14]. These included the MOF-adapted Revised Auto Correlations (RACs), and geometric descriptors. The heat capacity for each material was also used as a descriptor. Three gaussian regressors (one for each KPI: specific work, working capacity, and purity) were trained on these initial materials and the KPIs predicted for each material. The gaussian regressors then predict KPIs for all other materials, also returning an uncertainty. Using PyePAL, these predictions and uncertainties are used to classify materials as Pareto-optimal, discarded, or remain unclassified. A new material is then 'sampled' which involves using the TVSA model to return accurate KPIs. The gaussian models are then retrained. This process is iterated until all points have been classified. At the end of this iterative process, all points have been classified, and we have a Pareto-optimal material set, a sampled set, and the trained models. The sampled set and Pareto-optimal set are seen in Figure 4. The grey points are the material KPIs as calculated by the TVSA process and remain unsampled as they are not deemed relevant in the training of the regressors. In our case, we have sampled 195 materials (seen as the green points) out of 613. The points identified as Pareto-optimal are shown as red stars.

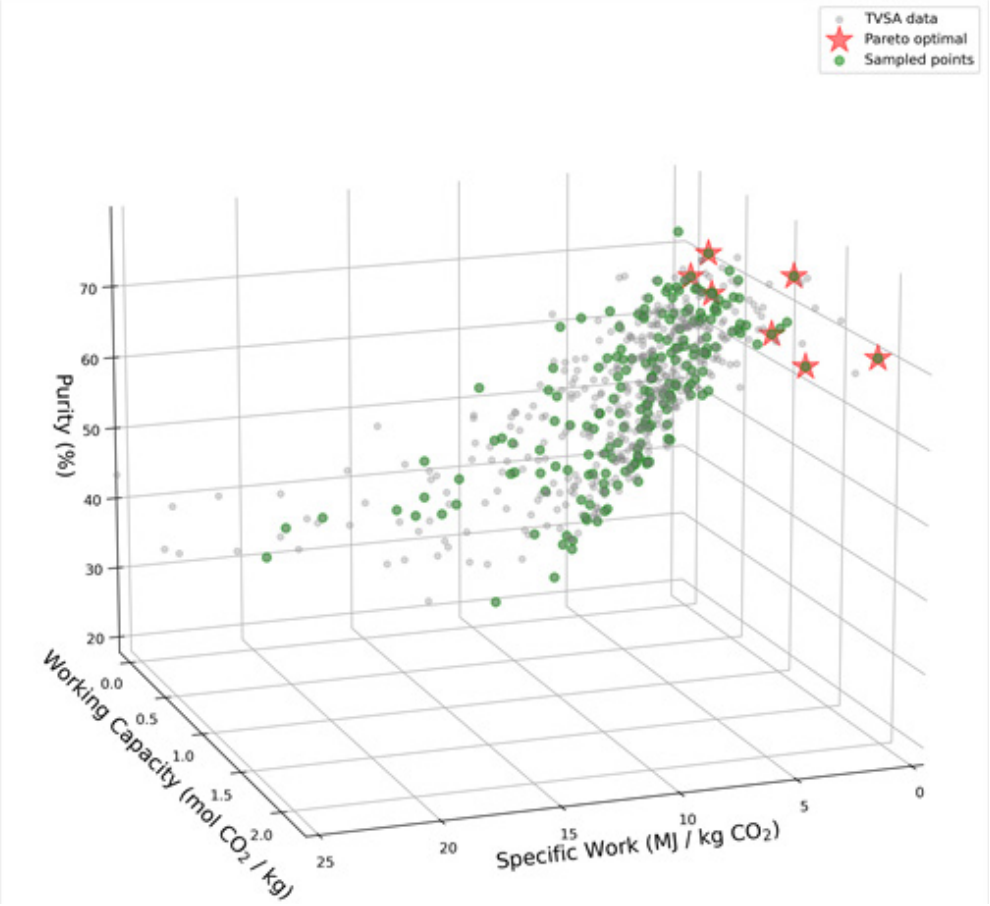


**Figure 4.** KPIs for each material as calculated by the TVSA process model are shown in grey. PyePAL samples points (green) as it builds a training set most relevant to Pareto-optimal materials (stars).

In terms of execution time, the brute-force technique where the TVSA model is used to calculate KPIs for all 613 materials takes 3 hours. Using PyePAL, only 195 materials are sampled which takes 1 hour. This time saving can be reduced further with a larger data set, as better predictive power from the regressors can be leveraged. As the number of MOFs within some databases venture into the trillions [15], time savings are increasingly important for MOF screening studies.

Future work with more materials will involve using the PyePAL algorithm to find important structure-property relationships. Specifically, we can discover what features are important to the regression models, as these give rise to good predictions for top-performers. In contrast, performing this analysis on a regression model trained without active learning would be biased towards the under-performing materials.

## Acknowledgments

This work is part of the PrISMa Project (299659), funded through the ACT Programme (Accelerating CCS Technologies, Horizon 2020 Project 294766). Financial contributions from the Department for Business, Energy & Industrial Strategy (BEIS) together with extra funding from the NERC and EPSRC Research Councils, United Kingdom, the Research Council of Norway (RCN), the Swiss Federal Office of Energy (SFOE), and the U.S. Department of Energy are gratefully acknowledged. Additional financial support from TOTAL and Equinor is also gratefully acknowledged. F.M. was supported by a James Watt Scholarship from the School of Engineering and Physical Sciences at Heriot-Watt University.

## References

[1] S. Sircar, T. C. C. Golden, and M. B. B. Rao, “Activated carbon for gas separation and storage,” *Carbon N. Y.*, vol. 34, no. 1, pp. 1–12, Jan. 1996.

[2] R. Anderson and D. A. Gómez-Gualdrón, “Deep learning combined with IAST to screen thermodynamically feasible MOFs for adsorption-based separation of multiple binary mixtures,” *J. Chem. Phys*, vol. 154, p. 234102, 2021.

[3] K. Nagesh Pai, V. Prasad, and A. Rajendran, “Generalized, Adsorbent-Agnostic, Artificial Neural Network Framework for Rapid Simulation, Optimization, and Adsorbent Screening of Adsorption Processes,” *Cite This Ind. Eng. Chem. Res*, vol. 59, 2020.

[4] Z. Yao *et al.*, “Inverse design of nanoporous crystalline reticular materials with deep generative models,” *Nat. Mach. Intell. 2021 31*, vol. 3, no. 1, pp. 76–86, Jan. 2021.

[5] K. Maik Jablonka, G. Melpatti Jothiappan, S. Wang, B. Smit, and B. Yoo, “Bias free multiobjective active learning for materials design and discovery.”

[6] P. G. Boyd *et al.*, “Data-driven design of metal–organic frameworks for wet flue gas $CO_2$ capture,” *Nature*, vol. 576, no. 7786, pp. 253–256, Dec. 2019.

[7] L. Riboldi *et al.*, “Advanced methodology for screening of novel adsorption materials for cost-efficient $CO_2$ capture,” *SSRN Electron. J.*, Mar. 2021.

[8] L. Joss, M. Gazzani, M. Hefti, D. Marx, and M. Mazzotti, "Temperature Swing Adsorption for the Recovery of the Heavy Component: An Equilibrium-Based Shortcut Model," *Ind. Eng. Chem. Res.*, vol. 54, no. 11, pp. 3027–3038, Mar. 2015.

[9] M. Zuluaga, A. Krause, and M. Püschel, "ε-PAL: An Active Learning Approach to the Multi-Objective Optimization Problem," *J. Mach. Learn. Res.*, vol. 17, pp. 1–32, 2016.

[10] A. L. Myers and J. M. Prausnitz, "Thermodynamics of mixed-gas adsorption," *AIChE J.*, vol. 11, no. 1, pp. 121–127, Jan. 1965.

[11] C. M. Simon, B. Smit, and M. Haranczyk, "pyIAST: Ideal adsorbed solution theory (IAST) Python package," *Comput. Phys. Commun.*, vol. 200, pp. 364–380, Mar. 2016.

[12] "Fidis – Scientific IT and Application Support - EPFL." [Online]. Available: https://www.epfl.ch/research/facilities/scitas/hardware/fidis/. [Accessed: 15-Jul-2021].

[13] S. Mohamad Moosavi *et al.*, "Understanding the diversity of the metal-organic framework ecosystem."

[14] Y. G. Chung *et al.*, "Advances, Updates, and Analytics for the Computation-Ready, Experimental Metal−Organic Framework Database: CoRE MOF 2019," 2019.

[15] S. Lee *et al.*, "Computational Screening of Trillions of Metal−Organic Frameworks for High-Performance Methane Storage," *ACS Appl. Mater. Interfaces*, vol. 13, 2021.

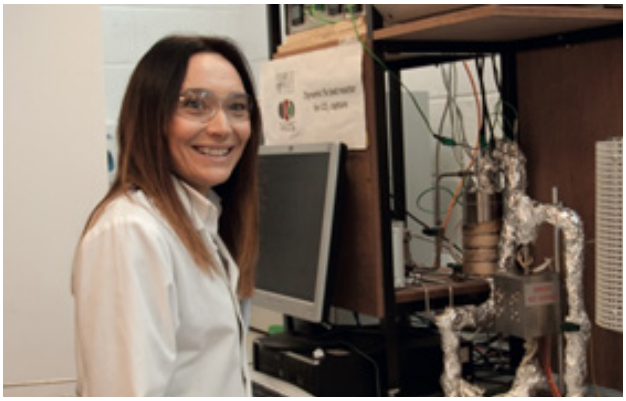

**Prof Susana Garcia**
Professor in Chemical Engineering
Associate Director in Carbon Capture and Storage,
Research Centre for Carbon Solutions (RCCS)

School of Engineering and Physical Sciences
Heriot-Watt University
Edinburgh, EH14 4AS
United Kingdom
Phone: +44 (0) 131 451 8083
Email: s.garcia@hw.ac.uk

***Susana García*** is Professor in Chemical Engineering and Deputy Head of the Institute of Mechanical, Process and Energy Engineering at Heriot-Watt University, which she joined in May 2014. She is also the Associate Director in Carbon Capture and Storage at the Research Centre for Carbon Solutions (RCCS), an interdisciplinary world leading engineering centre, inspiring and delivering innovation for the wider deployment of technologies needed to meet necessary carbon targets. She was the recipient of the Society of Spanish Researchers in the UK (SRUK/CERU) Emerging Talent Award 2020, in recognition of her outstanding professional trajectory, strong scientific outputs and mentoring and leadership qualities.

Her overarching research theme is the design and development of processes using advanced materials for specific applications relevant to energy efficiency and environmental sustainability in different sectors. She ambitions to change the paradigm on how novel processes based on advanced materials are developed through the integration of process engineering and basic science.

# Carbon nanomaterials for holography

## Nanomateriales de carbono para holografía

**María José Bañuls[1,2], Ángel Maquieira[1,2], María Isabel Lucío[1,*]**

*[1]Instituto Interuniversitario de Investigación de Reconocimiento Molecular y Desarrollo Tecnológico (IDM), Universitat Politècnica de València, Universitat de València, Camino de Vera s/n, 46022 Valencia, Spain.*

*[2]Departamento de Química, Universitat Politècnica de València, Camino de Vera s/n, 46022 Valencia, Spain.*

**Corresponding author: malube@upv.es*

### Abstract

Holography is a technique to produce and store three dimensional images. It has awakened special interest since its inception as it has applications in several field such as the production of security labels, the development of sensor, in massive storage or in metrology and microscopy. Holography is based on the recording of interfering patterns onto photosensitive materials thus creating a hologram. The light employed as well as the composition of the photosensitive materials are key elements to produce holograms of high quality.

Due to their interesting electrical and optical properties, carbon nanomaterials have been widely studied for the fabrication of holograms of advanced properties.

This review summarizes the use of carbon nanomaterials in holography. A short introduction of the types of holograms as well as the most common photosensitive materials is described. Finally, the emerging of new technologies different to holography for the fabrication of diffractive materials based on carbon nanomaterials is briefly presented.

### Introduction

Classical photography involves the illumination of an object with light (sunlight or artificial) and the register of the diffused light by the object in a photographic plate composed of a photosensitive material (usually a gelatine that contains halide salts) that is modified by the action of the light coming from the object. The magnitude of the modification is proportional to the intensity of the emitted light by the object. After the adequate treatment of the photographic plate (developing, fixation and washing), it will have bright and dark zones related with shape of the object. However, as only the intensity is registered, the photograph will be a two-dimensional image of the object.

Looking for an improvement in the resolution of the electronic microscopy, holography appeared in the forties as a technique to produce and store three dimensional images.[1] It was first described by Dennis Gabor, who was awarded the Nobel Prize for Physics in 1971 for its discoveries.

Holography entails two steps, recording and reconstruction.[2] In the recording process, a photosensitive material is illuminated with a reference beam and the emitted wavefront from the object (object beam), in such a way that the two waves interfere at the surface of the material (Figure 1 A), thus becoming a hologram. After the adequate postprocessing treatment, if needed, the hologram contains fringes of bright and dark zones, similar to a photography; but thanks to the interference of the two beams, it contains information about the phase and amplitude of the registered wave and not only about the intensity of the light. In the reconstruction stage, the hologram is illuminated with a light beam, similar to the reference one, and the diffracted light generates the three-dimensional image of the object (Figure 1 B).

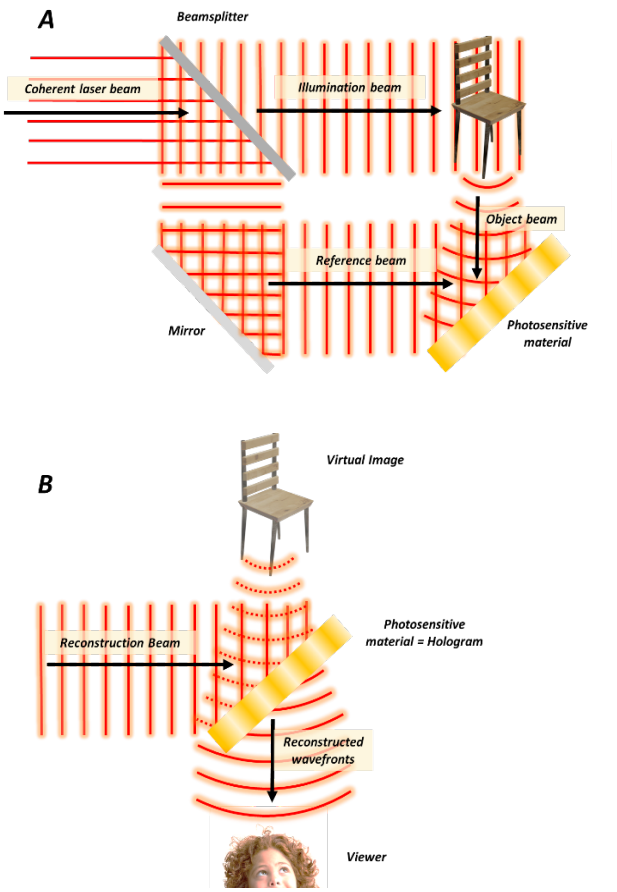


**Figure 1.** Holographic process steps: **A)** Recording and **B)** Reconstruction.

Although initially holography arose as a technique to register or store images, since its discovery, it has found applications in multiple fields such as virtual reality,[3] storage of information,[4] optical waveguides,[5] solar concentrators,[3] memories,[6] sensors,[7] holographic microscopy[8] or holographic spectroscopy.[9]

However, despite its great potential, real applications of holography have not totally taken off as the process requires certain requirements that still have ample room for further improvements. On one hand, the interfering waves should be coherent (the phase difference between them should be constant); and on the other hand, the photosensitive material that is modified by these waves should has high resolving power. This property is defined as the capacity of the material to distinguish the spatial frequencies of the interference pattern. That is, to correctly differentiate the bright and dark zones of the light that will eventually form the fringes of the hologram. The problems related with the coherence of light were solved with the discovery of lasers in 1962, and the ones related with the resolution of the materials are step by step being overcome with the development of new photosensitive materials.

Silver halide sensitized gelatines, dichromated gelatine, photothermoplastics, photopolymers, photoresist and photorefractives have been used as photosensitive materials for storing holograms. Concretely, photopolymers highlight among other systems as they do not require complicated post-recording chemical treatments to form the hologram. Indeed, hologram is created in situ during the recording process, thus, photopolymers are self-processing. Other interesting materials are photorefractives, defined as any material that changes its refractive index under illumination due to electronic processes. The most interesting advantages of photorefractives is that they can be used for read-write applications (as they are optically “erasable”) and in real-time holographic display, and do not require high optical power density to be processed. Photorefractive can be inorganic crystals or organic compounds, but liquid crystals stand out due to their high sensitivity to optical field as well as for their capacity to supply the hologram with superior properties. Nonetheless, photopolymers and liquid crystals materials are not absent of drawbacks and numerous research efforts are aimed to improve them in terms of increasing their resolving powers, diffractive efficiencies, or response rates. Different strategies are being addressed to get these objectives. Among them, some of the most interesting are their use in conjunction, thus called polymer-dispersed liquid crystals (PDLC),[10] and their doping with carbon nanomaterials.

Carbon nanomaterials have a noticeable standing among all the nanomaterials owing to the combination of dimension, structure and topology that translates into exceptional electrical, thermal, chemical, and mechanical properties. In holography, carbon nanomaterials are used to provide the photosensitive materials with superior properties due to their high refractive index and conductivity.

Here, we review the types of holograms, the use of photopolymers and photorefractive as photosensitive holographic materials and their doping with carbon nanostructures for the improvement of their performance. Finally, the use of carbon nanostructured to directly create holograms will be briefly discussed.

## Types of holograms

Holograms can be classified according to different criteria. On one hand, the classification can be carried out according to the properties of the incident light that are modified after the recording: the phase or the amplitude. When light hits the photosensitive material, it can modify its refractive index (n) or its thickness (d), thus becoming a phase hologram; or its absorption coefficient (α), thus becoming an amplitude hologram. Another classification responds to the physical characteristics of the hologram. In volume or thick holograms, the thickness of the recording material is much larger than the average spacing of the created fringes, while in surface or thin holograms, the thickness is negligible versus the fringe period. Finally, they can be classified as reflection or transmission holograms depending on the geometry of the holographic recording, that is, the direction of the recording laser beams. In transmission holograms, the two interfering laser beams enter the material from the same side, hence the fringes are perpendicular to the surface of the material (Figure 2 A). In reflection holograms the two interfering laser beams hit the material from their two opposite sides, thus fringes are parallel to the surface of the material (Figure 2 B).

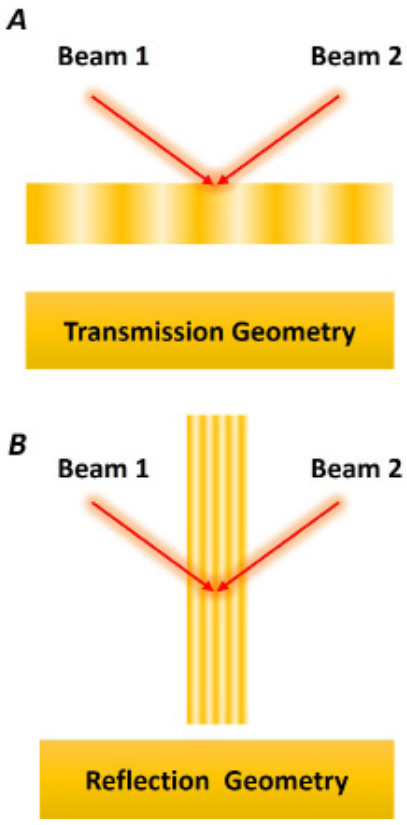


**Figure 2.** Formation of **A)** a transmission hologram and **B)** a reflection hologram.

## Fabrication of holograms with photopolymers and liquid crystals

Photopolymers are materials that polymerize by the action of light at a specific wavelength. In

holography, photopolymers are normally composed of one or several monomers and crosslinkers, a photoinitiator and a plasticizer, all embedded in a binder (polymerized inert matrix). They are usually disposed as a film of specific thickness over a flat surface. Then, they are illuminated with the interfering beams to record the hologram. During the recording process, light provokes the polymerization of the monomers in the bright zones thanks to the photoinitiator. As the polymerization evolves, a simultaneous migration of monomers from the dark zones is produced. At the end of the register process, the fringes of the holograms consist of polymerized and non-polymerized zones that differ in their refractive index; consequently, phase holograms are created (Figure 3). As one can envision, multiple variables can affect to the hologram formation, since the characteristics of the recording process by itself (laser power, time, geometry, etc) to the composition of the photopolymers (kind and concentration of the reagents).

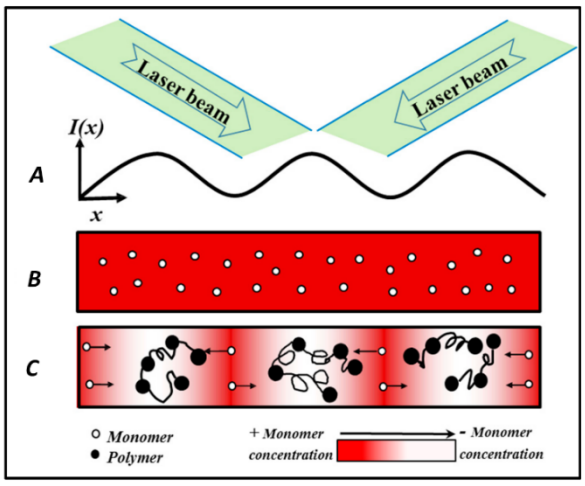


**Figure 3.** Formation of gratings in a photopolymer material: **A)** the sinusoidal illuminating intensity distribution at the plate; **B)** the uniform photopolymer before recording; and **C)** the photopolymer during recording (mass transport and polymer chains). Reprinted with permission from *Polymers* **2017**, *9*(8), 337. Copyright © 2017, MDPI.

In polymer-dispersed liquid crystals, photopolymers are doped with liquid crystals forming a homogeneous material. In this way, when polymerization is taking place and monomers are migrating from dark to bright zones, a concurrent relocation of the liquid crystals from the bright to the dark zones is generated, where they remain as droplets (Figure 4 A). This process is called photo-polymerization induced phase separation process and the photosensitive material for the formation of the holograms is called H-PDLC (Holographic Polymer-Dispersed Liquid Crystals). Apart from the improvement of the structural consistency of the layer, the decrease in the shrinkage processes, and the increase in the refractive index modulation of the holograms, the hallmark of the H-PDLC is that, due to the optical anisotropy introduced by the liquid crystals, the holograms adopt new electro-optical properties, and their response can be modified by the application an external electric field. That means that the electrical field can modify the diffraction efficiency of the hologram, so it can be useful for the development of optical switching devices. The modification is produced by the reorientation of the LC droplets within the electric field (Figure 4 B).

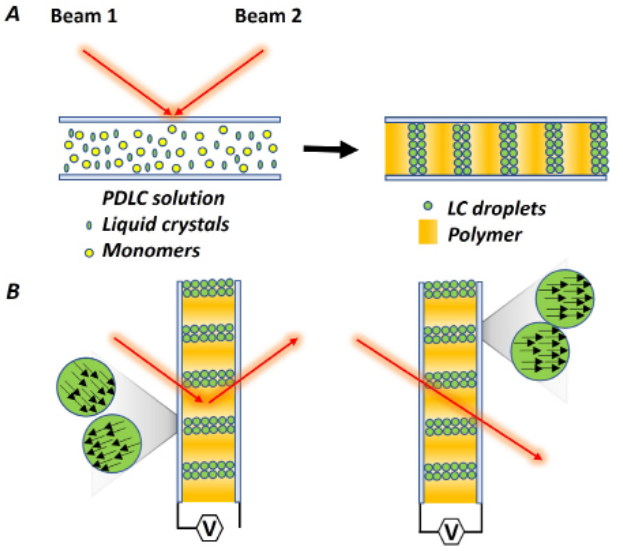


**Figure 4. A)** Formation of gratings in a solution of PDLC: Photopolymerization takes place in bright zones while LCs migrate to dark zones as droplets. **B)** Detailed scheme of the reorientation of the LC droplets in gratings in the presence of an external electric field. When the voltage is off the light is diffracted, while it is transmitted when the voltage is on.

## Carbon nanostructures as additives in holographic photopolymers

Carbon nanomaterials have been added to photopolymers mainly to generate a higher modulation of the refractive index in the photosensitive materials with the aim of increasing their diffraction efficiency. Tomita et al. added nanodiamonds (NDs) to photopolymers to increase the modulation of the refractive index (Δn) of the material and, thus, improve its diffraction efficiency.[11] They fabricated unslanted volume transmission holograms with the monomers tri- and tetrapentaetrythritol acrylate and a single functional ionic liquid monomer dopped with NDs at different proportions. Photopolymerization, triggered by the interfering waves, causes a migration of the NDs to the dark zones while photopolymer is formed in the bright zones, thus increasing the refractive index modulation. In addition, they performed slow-neutron diffraction experiments, observing that the fabricated gratings were excellent candidates for their use in neutron optics as they showed DE > 20 % (Figure 5). In a recent study, Guo et al. incorporated single-walled carbon nanotubes (CNTs) in a mixture of trimethylolpropane triacrylate (TMPTA), trimethylolpropane tris(3-mercaptopropionate) (TMPTMP), and 1,3,5-triallyl-1,3,5-triazine-2,4,6(1H,3H,5H)-trione (TATATO) to fabricate volume transmission holograms.[12] They observed how the CNTs not only promote and accelerate the allylic polymerization of the monomers

but also increased the refractive index modulation of the holograms which generated high diffraction efficiencies (>96%). In addition, CNTs improved the mechanical properties of the holograms without compromising their flexibility. Chen et al. studied the effect of the addition of graphene oxide sheets in a methyl methacrylate (MMA) mixture.[13] The fabricated holograms with this mixture proved how the graphene oxide contributed positively to the enhancement of the diffraction efficiency by promoting the polymerization of MMA. The experimental results also showed that the graphene oxide was grafted to the polymers chains which could benefit the refractive index modulation of the photosensitive material.

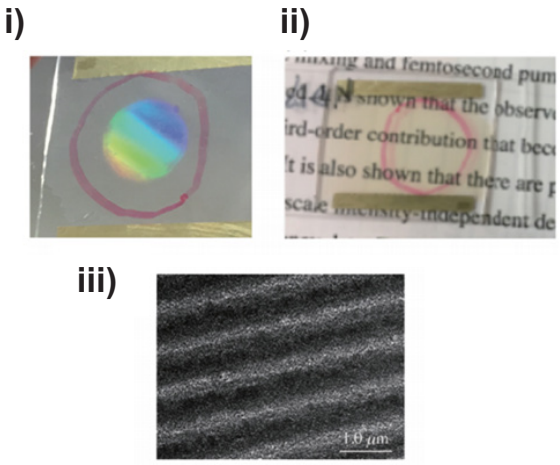


**Figure 5.** Hologram fabricated with photopolymers doped with nanodiamonds by Tomita et al. i) Photograph of the hologram under illumination with white-light, ii) Photogram of the same hologram viewed from the top and iii) from a fluorescent lamp and iii) TEM image of the cross section of the grating. Reprinted (adapted) with permission from *Phys. Rev. Appl.* **2020**, *14* (4), 1. Copyright © 2020, American Physical Society.

## Carbon nanomaterials as additives in holographic PDLC

Carbon nanomaterials have been added to H-PDLC mainly to improve the electrical conductivity of the holograms and, thus, to decrease the voltage needed to perturb their optical responses. Fullerenes were introduced into PDLC by Kim[14] to increase the electrical conductivity of polymer matrixes and hence the local electric field on LC droplet. This led to a decrease in the droplet size of the LC, with increased droplet density, that was translated into an augmented diffraction efficiency while the operating voltage was reduced. Later, same authors studied the doping of PDLC with multi-walled carbon nanotubes observing that the diffraction efficiency was increased due to the induced local electric field of the polymer but also to the delay in the nucleation of LC during the periodic modulation. Interestingly, they carried out the experiments with pristine and vinyl-modified CNTs, observing better performance of the functionalized ones ascribed to their finer dispersion. Surprisingly, larger LC droplets were observed with the functionalized CNTs.[15] A different group observed that CNTs play the same role when they were incorporated in different polymer matrixes (Figure 6).[16,17]

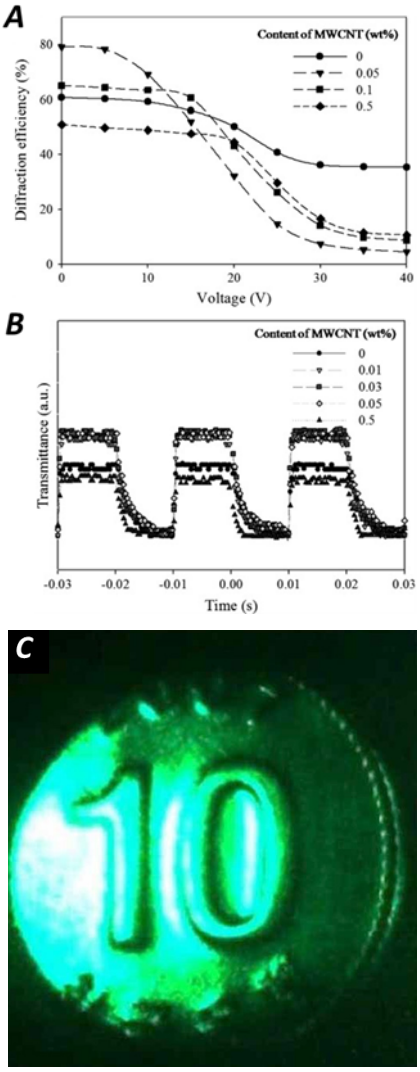


**Figure 6.** Electro-optical properties of the H-PDLC obtained by Kim et al. using a polyurethane-based matrix doped with various MWCNT contents at 40 wt% LC: **A)** driving voltage and **B)** response time at 50 Hz, 30 V**. C)** Photograph showing a reconstructed virtual image of a coin recorded using a H-PDLC obtained at 40 wt% LC with 0.05 wt% MWCNTs. Reprinted (adapted) with permission from *Polym. Int.* **2010**, *59* (9), 1289–1295. Copyright © 2010, John Wiley and Sons.

In a posterior study, similar results were observed with graphene as it improved the local electric field and the diffraction efficiencies of PDLC.[18] However, while polymer conductivity increased linearly with the increasing graphene content, excessive quantities of graphene (higher than 0.10 %) produced undesired augmented viscosity and aggregation processes detrimental of the diffraction efficiency. The same studies performed with allyl-modified graphene oxide confirmed the role of the graphene in the viscosity, the grating kinetics and morphology, the diffraction efficiency (DE), and the electro-optical properties of holographic PDLC.[19] The group of Fontecchio also doped the PDLC with oxidized multi-walled carbon nanotubes observing a decrease of the LC droplet sizes and improved electro-optical response of the holographic material leading to increased diffraction efficiencies.[20,21] In an interesting study, multiwalled carbon nanotube were covalently functionalized with liquid crystal chains and subsequently used to dope PDLCs.[22] The functionalization improved dispersion

of the CNTs in the medium which yielded holograms with enhanced electro-optical properties in terms of voltage requirements. In the last study found about this topic, Liu et al. doped PDLCs with multiwalled carbon nanotubes and carried out theoretical simulations to analyse and predict the effect of the CNTs on the electro-optical properties of the holograms.[23]a model developed for establishing the lowest possible driving voltage of Holographic polymer-dispersed liquid crystal (H-PDLC They showed how the CNTs improved the phase separation of LC and polymer regions and accumulated in the LC region, thus improving the diffraction efficiency of the holograms. CNTs also modified the LC droplet sizes and decreased the dielectric permittivity of the gratings that improved their electro-optical response. One of the problems of holograms fabricated with liquid crystal is that they are not temporally stable. However, Abbasov et al. proved that the doping with carbon nanotubes could not only improve the diffraction efficiency of liquid crystal-based holograms but also improve their stability over time (over two years).[24] Gao et al. also doped liquid crystal films with carbon dots observing good diffraction efficiencies with low voltages.[25] What is more, they acquired real-time dynamic holographic display videos with these films which might be potentially applied in future true 3D TV display.

### Fabrication of holograms by the laser ablation of carbon nanomaterials

Holograms have also been generated by the direct photoreduction of graphene oxide.[26] Li et al. dispersed graphene oxide into polyvinyl alcohol binder and spin coated the solution over a glass slide to create a thin film. By the application of fs-pulsed laser beam at the wavelength of 800 nm, they were able to reduce the graphene oxide and thus, create holographic gratings. What is more, they observed that they could modulate the phase of the materials by changing the pulse fluence of the laser beam. The large dynamic range of the phase modulation opened the door to the fabrication of holograms of high diffraction efficiency able to generate three-dimensional holographic images with a wide viewing angle.

### Patterns of carbon nanomaterials with applications in holography

Butt and others have used carbon nanomaterials to fabricated diffractive elements useful as holograms in processes alternative to holography. They fabricated uniform patterns of nanomaterials onto transparent support via electron-beam technologies in such an ordered way that they could diffract light as holograms do (Figure 7). The most interesting property of these diffractive elements is that, due to the nanoscale dimension of nanomaterials, they can generate diffraction images of high contrast and with very large field of view. Carbon nanotubes have been the main carbon nanomaterial employed for the fabrication of these kind of diffractive elements[27–31] but they have also used graphene obtaining very good results.[32] Although the technique developed by Butt and co-workers awaken interest in holography, it will not be deeply discussed here as their technology would deserve a different perspective of analysis as it is not holography in terms of using beam interference.

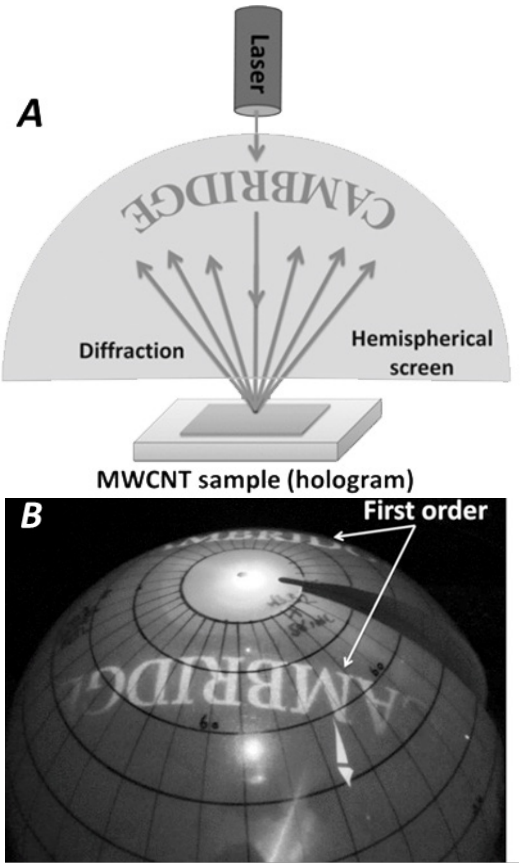


**Figure 7.** Experimental setup and measured diffraction pattern results of the holograms fabricated by Butt and colleagues. **A)** The schematic diagram of the experimental setup employed to capture the diffraction pattern. **B)** The pattern was obtained on a semitransparent hemispherical screen of radius 15 cm by shining a green (532 nm) laser perpendicular to the plane of the CNT array. A clear CAMBRIDGE image was observed in the first order of the diffraction pattern.

### Future perspectives

Holography is an advanced technology useful in multiple fields. The laser interference warrants an accurate control of the fabrication processes in terms of holograms dimensions. However, to exploit all its potentials, the improvement of the holographic materials is still needed. This review has summarized the use of carbon nanomaterials to improve the performance of the photosensitive materials used for the recording of holograms. In addition, it has presented the fabrication of diffractive patterns of carbon nanomaterials that could be used as holograms using alternative technologies. The studies here presented show how holography benefits from the excellent properties of the carbon nanomaterials in many ways, such as improvement of mechanical and elecro-optical properties of the gratings or enhancements in their diffraction efficiencies. Nonetheless, despite all the efforts, there is still room for improvement in this research area.

For example, a total control over the functionalization of the carbon nanomaterials to improve the viscosity and conductivity of the photopolymers seems to be absolutely needed. This could imply using different functional groups and methodologies to increase the length of the organic chains attached to the nanomaterials. In addition, it should be noticed that carbon nanomaterials are presented in multiple formats (size and shapes) and not all of them have been studied. New studies about the anchoring of the nanostructured to the photopolymers would also be beneficial for understanding the mechanisms of the grating formations.

**Acknowledgements**

This work was financially supported by the E.U. FEDER, the Spanish Ministry of Economy and Competitiveness MINECO (AdBiHol-PID2019-110713RB-I00) Generalitat Valenciana (PROMETEO/2020/094). M. I. Lucío acknowledges MINECO for her Juan de la Cierva-incorporación grant (IJC2018-035355-I).

**References**

[1] Gabor D, Nature 1948; 161: 777-778.

[2] Beléndez A, Fundam. Óptica Para Ing. Inform., Servicio De Publicaciones De La Universidad De Alicante, 1996.

[3] Chen Z, Lin Q, Li J, Yu X, Gao X, Yan B, Wang K, Yu C, Xie S, Opt. Commun 2017; 384: 125-129.

[4] Ortuño M, Gallego S, Márquez A, Neipp C, Pascual I, Beléndez A, Materials 2012; 5: 772-783.

[5] Malallah R, Li H, Kelly DP, Healy JJ, Sheridan JT, Polymers 2017; 9: 337.

[6] Ortuño M, Gallego S, García C, Neipp C, Beléndez A, Pascual I, Appl. Phys. B Lasers Opt 2003; 76: 851-857.

[7] Yetisen AK, Naydenova I, Da Cruz Vasconcellos F, Blyth J, Lowe CR, Chem. Rev. 2014; 114: 10654-10696.

[8] VanLigten RV, Osterberg H, Nature 1966; 211: 282.

[9] Bräunchle C, Burland DM, Angew. Chemie - Int. Ed 1983; 22: 582-598.

[10] Fenoll S, Brocal F, Segura JD, Ortuño M, Beléndez A, Pascual I, Polymers 2019; 11: 325.

[11] Tomita Y, Kageyama A, Iso Y, Umemoto K, Kume A, Liu M, Pruner C, Jenke T, Roccia S, Geltenbort P, et al, Phys. Rev. Appl 2020; 14: 1.

[12] Guo J, Cao L, Jian J, Ma H, Wang D, Zhang X, Carbon 2020; 157: 64-69.

[13] Chen Y, Hu P, Huang Z, Wang J, Song H, Chen X, Lin X, Wu T, Tan X, ACS Appl. Mater. Interfaces 2021; 13: 27500-27512.

[14] Matsumura S, Hlil AR, Lepiller C, Gaudet J, Guay D, Shi Z, Holdcroft S, Hay AS, J. Polym. Sci. Part A Polym. Chem. 2008; 46: 7207-7224.

[15] Sun KR, Kim BK, Polym. Adv. Technol. 2011; 22: 1993-2000.

[16] Kim EH, Lee JH, Jung YG, Paik U, Polym. Int. 2010; 59: 1289-1295.

[17] Lee W, Chen HY, Yeh SL, Opt. Express 2002; 10: 482.

[18] Kim BK, Jang MW, Park HC, Jeong HM, Kim EY, J. Polym. Sci. Part A Polym. Chem. 2012; 50: 1418-1423.

[19] Jang MW, Kim BK, J. Mater. Chem. 2011; 21: 19226-19232.

[20] Shriyan SK, Fontecchio AK, Mol. Cryst. Liq. Cryst. 2010; 525: 158-166.

[21] Shriyan SK, Fontecchio AK, Opt. Express 2010; 18: 24842.

[22] Wu Y, Cao H, Duan M, Li E, Wang H, Yang Z, Wang D, He W, Liq. Cryst. 2018; 45: 1023-1031.

[23] Liu Y, Shen J, Shen T, Zheng J, Zhuang S, J. Mater. Sci. 2021; 56: 12660-12670.

[24] Abbasov ME, Ghosh S, Quach A, Carlisle GO, J. Mater. Sci. Mater. Electron. 2010; 21: 854-859.

[25] Gao H, Li S, Liu J, Zhou W, Xu F, Dai Z, Cheng X, Fang H, Ge X, Sun L, Mater. Express 2020; 10: 780-787.

[26] Li X, Ren H, Chen X, Liu J, Li Q, Li C, Xue G, Jia J, Cao L, Sahu A, et al., Nat. Commun. 2015; 6: 1-7.

[27] Butt H, Montelongo Y, Butler T, Amaratunga GAJ, Wilkinson TD, 2013 Saudi Int. Electron. Commun. Photonics Conf. SIECPC 2013, 8-11.

[28] Butler TP, Butt H, Wilkinson TD, Amaratunga GAJ, Nanoscale 2015; 7: 13452-13457.

[29] Butler TP, Rashid I, Montelongo Y, Amaratunga GAJ, Butt H, Nanoscale 2018; 10: 10683-10690.

[30] Butt H, Montelongo Y, Butler T, Rajesekharan R, Dai Q, Shiva-Reddy SG, Wilkinson TD, Amaratunga GAJ, Adv. Mater. 2012; 24: 331-336.

[31] Montelongo Y, Chen B, Butt H, Robertson J, Wilkinson TD, Appl. Phys. Lett. 2013; 103: 111104.

[32] Butt H, Kidambi PR, Dlubak B, Montelongo Y, Palani A, Amaratunga GAJ, Hofmann S, Wilkinson TD, Adv. Opt. Mater. 2013; 1: 869-874.

**María Isabel Lucío** received her BSc degree in Chemistry and her MSc degree in Green Chemistry at the University of Castilla-La Mancha (UCLM). Later, she carried out her PhD at the University of Trieste and the UCLM. After her postdoctoral stays at the Nanomedpharma Ltd. company and the University of Southampton, she joined the Polytechnical University of Valencia (UPV) thanks to a Juan de la Cierva-Formación grant. Currently, she holds a Juan de la Cierva-Incorporación position at the same university. Her research interests are focused on the synthesis of new bioresponsive hydrogels, with special emphasis on their optimization for the development of holographic materials useful in optical biosensing.

# Carbon-based nanomaterials for skin-related applications

## Nanomateriales de carbono para aplicaciones relacionadas con la piel

**Cristina Martín**[1*]

[1] *Dpto. de Bioingeniería en Ingeniería Aeroespacial, Universidad Carlos III de Madrid Avda. de la Universidad, 30. 28911 Leganés (Madrid)*

**Corresponding Author: cristima@ing.uc3m.es*

**Abstract**

Skin is the largest organ of the body and the first protective barrier to the environment, playing a crucial role in covering other organs and also as a health state indicator. In this review, we describe the benefits of using carbon-based nanomaterials (CBN) for skin-related applications, focusing on carbon nanotubes (CNT) and graphene derivatives. Tactile, temperature and humidity sensors containing these nanomaterials, as well as advanced devices for health monitoring are discussed. Furthermore, the biodegradation and the biomedical applications, such as skin cancer treatment, of carbon nanomaterials-based hybrids are summarized over the manuscript.

### 1. Introduction

Human skin is the largest sensory organ of the body. It is one of the best indicators of health condition and it acts as an environmental barrier to protect other organs. Human skin consists of epidermal, dermal, and subcutaneous layers, all connected by a complex vascular nervous network [1]. In addition, skin has a well-developed stroma, which has neurosensory properties where receptors sense touch, pain, and heat stimuli [2,3].

The unique structural dimensions and excellent physicochemical properties of carbon-based nanomaterials (CBN), including fullerenes, carbon nanotubes (CNT), graphene and its derivatives, nanodiamonds and carbon dots, make them extremely interesting materials [4]. These extraordinary properties (i.e. electrical, mechanical, thermal, catalytic, and electrochemical properties) encourage the use of CBN in diverse areas, including biomedical engineering [5]. Because of their abundance and low production cost, CBN have been considered for replacing other conventional materials, such as the Si-based ones, in order to develop novel smart devices with high-temperature stability, high electrical conductivity or enhanced mechanical properties, among others. In parallel, the great development of soft materials has enabled a precise modulation of 3D scaffolds' properties so they are quite similar to those of the mimicked organ of interest, including skin [6].

In such context, the so-called "skin-inspired electronics" [7] and more precisely, stretchable electronic skin (e-skin), has attracted a high degree of interest due to its ability to detect subtle stimuli changes, and undoubtedly, CBN play a crucial role on the design of such cutting-edge devices. In particular, e-skins based on graphene derivatives have experienced a huge progress in the last few years with the development of advanced tactile [8,9], temperature [10], or humidity [11] sensors, and also regarding multimodal e-skin [12] or health-care monitoring [13]. Considering the high number of articles published in the skin-related field using CNT and graphene derivatives, in this review we will mainly focus on both kinds of CBN.

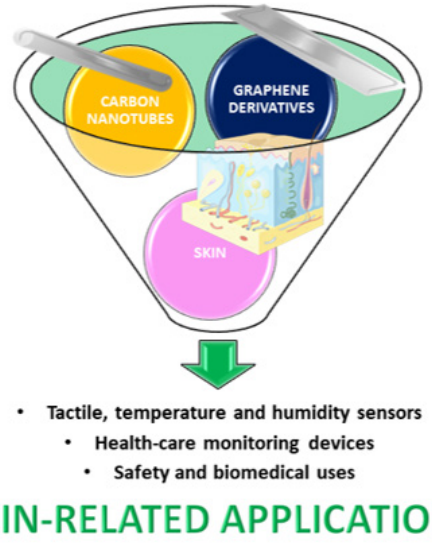


**Figure 1**. Carbon nanotubes and graphene derivatives for skin-related applications.

### 2. Tactile, temperature and humidity sensors

Since the moment a prosthetic hand with tactile feedback was reported by Clippinger *et al*. in 1974, [14] multiple investigations have been carried out to study the enormous application of tactile bionics [15,16]. The piezoelectric property of some anisotropic materials is known to convert mechanical forces into electrical charges due to the occurrence of electrical dipole moments. Due to the excellent electrical conductivity and good flexibility properties of CNT and/or graphene-related materials, a tiny stress deformation applied on these sensors can lead to a dramatic change of resistance. Thus, this ability has been used for the generation of multiple bioinspired tactile sensors based on carbon-related materials, that are able to undertake similar tasks to that of human skin, namely the sensing of external stimuli such as pressure, strain and torsion [17–19]. Lipomi *et al*. [20] developed a skin-like pressure and strain sensor based on transparent elastic films of CNT. Another example is the work reported by Lou *et al*., [21] who manufactured an ultra-sensitive and

rapid response speed graphene pressure sensor with a highly reproducible electrical response to repetitive 100,000 loading-unloading cycles of 500 Pa. CNT and reduced graphene oxide (rGO) were also used together to manufacture composite nanofibers for ultraflexible, optically transparent and piezoresisitive pressure sensor arrays [22]. The device could be attached on the surface of human skin or other soft movable scaffolds to precisely monitor the pressure distribution, showing a negligible crosstalk thanks to the 1 mm spacing between sensor arrays.

Regarding the mimicking of the temperature-sensing ability in skin to help maintaining the thermal equilibrium between human body and ambient environments, multiple temperature sensors containing CBN have been developed [9,18,23–25]. Temperature-dependent resistance variations can be measured through the temperature coefficient of resistance (TCR = (ΔR/R)/ΔT) [9,26]; the temperature dependence of sensitive rubbers, for instance, depends on the concentration and type of filler: CNT-filled rubber displays decreasing resistance with increasing temperature, while graphene–filled rubber displays the opposite trend. However, by co-dispersing both CNT and graphene in an elastomer matrix, the temperature sensitivity of the composite resistivity can be eliminated [27].

which usually display a negative temperature coefficient. An interesting example could be the work reported by Ko and co-workers [30], who designed a human-skin-inspired temperature sensor based on rGO sheets. They confirmed a typical negative temperature coefficient behavior with a high TCR of 2.93 %/ºC, that could be attributed to the changes of contact resistance among the rGO sheets by thermomechanical changes. In this case, the sensor also had the capacity to detect the temporal response to cycling temperature variations.

Monitoring the water concentration coming from the human body or its surroundings is convenient for personalized healthcare. In such direction, pressure, temperature or humidity sensors containing CBN, that can be wearable or adhesive to human skin, have been developed [31,32]. The advantages in this case over other materials are more notable, since commercially available porous ceramics for humidity sensing are normally stiff and fragile [33]. In the case of humidity sensors, graphene derivatives are the most promising candidates due to its hygroscopic characteristic and large specific surface area. Typically, the performance mechanism of graphene-based humidity sensors is ascribed to the influence of vapor molecules on the charge carrier density of the nanomaterial, resulting in the resistance variation of the graphene sheets.

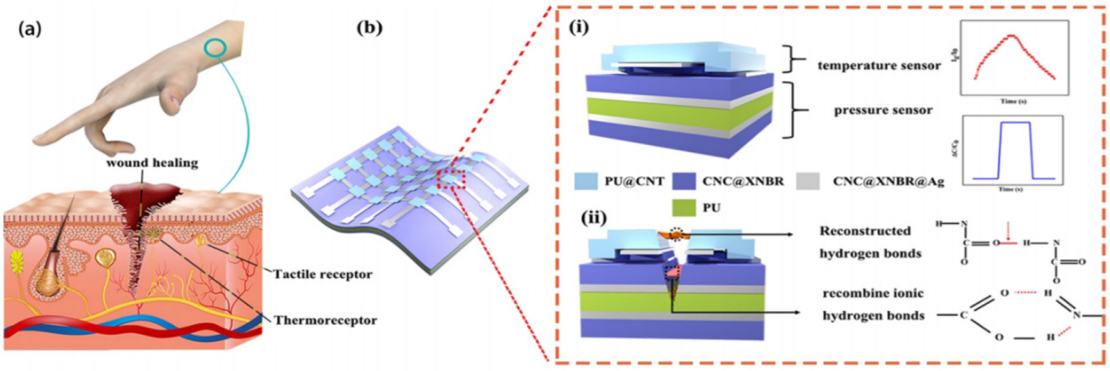


**Figure 2**. (a) Scheme of the human tactile receptors and temperature receptors with self-healing properties. (b) Scheme of the developed self-healable bifunctional e-skin. Adapted with permission from [28]. Copyright 2020 American Chemical Society.

Shen and co-workers [28] have recently reported a bifunctional self-healing e-skin with stacked integrated capacitive pressure and resistive temperature sensors based on polyurethane and multiwalled CNT (Figure 2). As a semiconductor, CNT with negative temperature coefficients stimulate electrons to enter the conduction band with increasing temperature, resulting in a resistance decrease. Even microfluidic sensors using CNT [24] or graphene derivatives [29] have been manufactured for sensing temperature and/or pressure. Graphene has ultrahigh thermal conductivity and unique sensitivity to temperature changes. Moreover, it shows a lower convective heat-transfer coefficient compared to metals and CNT, resulting in a higher final temperatures and faster heating rates. Because of these features, in the last few years, graphene has been extensively applied in flexible and stretchable temperature sensors,

In the case of rGO, the resistance of the nanomaterial can be increased, since water molecules can be adsorbed at the residual functional groups of the surface. In general, humidity can create distance changes between adjacent graphene oxide (GO) layers in a reversible way. The main problem regarding these systems is the generation of sufficiently flexible and stretchable devices keeping a high sensitivity. In this context, a sensing graphene/polypyrrole material was created by Wu and co-workers [32], reaching response and recovery times of approximately 15 s and 20 s, respectively, and a high humidity sensitivity. In another work, a humidity sensor based on rGO and polyurethane has been recently reported [34]. Here, the authors highlighted the maintenance of the sensitivity under high stretching state of 60% strain after 10,000 stretching cycles. An interesting example is the work developed by Sreeprasad *et al*. [35], who

used graphene quantum dots and demonstrated a high humidity sensitivity by a mechanism governed by those graphene quantum dots, selectively interfaced with polyelectrolyte microfibers forming an electrically percolating-network.

Nevertheless, physiologically skin-to-skin contact induces a simultaneous temperature and humidity variation, and moreover, a tactile stimulus occurs on human skin at the same time. This means that e-skin should be designed to sense multiple stimuli in order to really mimic human skin, which is known as "multimodal e-skin". Park *et al*. [30] developed microstructured ferroelectric skins containing different concentrations of rGO that could detect and discriminate between multiple spatiotemporal tactile stimuli. The authors demonstrated the applicability of these sensors by the simultaneous monitoring of pulse pressure and temperature of artery vessels. Shortly after, a stretchable and multimodal "all graphene" electronic skin was reported [36]. Humidity, thermal and pressure functional sensors were included in that matrix and were judiciously integrated into a layer-by-layer geometry through a simple lamination process. Concerning CNT, a highly sensitive and multimodal skin sensor which was capable of simultaneously detecting tactile and biological stimuli was developed [37]. In this case, a wearable and multimodal skin sensor using CNT fabrics was capable of sensing external stimuli such as tactile, temperature, humidity at the same time, and even discern input signals derived from versatile chemical fluids with different dipole moments.

It is important to highlight the opportunity offered by printing techniques, perfect tools to generate a variety of solution-based materials on polymeric substrates over big areas for multifunctional electronics [38,39].

### 3. Health-care monitoring devices

The increasing necessity for patient-friendly therapies together with the rise in medical costs arising from the population aging and an increment in chronic diseases, have sparked the development of skin-mountable therapeutics and drug delivery systems that are more efficient and easier to use than conventional techniques [1]. These devices provide point-of-care services at home, thereby potentially reducing primary care patient load. Salvatore and co-workers [40] thoroughly reviewed in 2017 the concept of "lab-on-skin" to describe a variety of electronic devices with physical properties similar to those of skin and that are able to provide accurate, non-invasive, long-term and continuous health monitoring.

Stretchable CNT strain sensors for human-motion detection were reported in 2011 [41]. The authors assembled the CNT sensors on stockings, bandages and gloves in order to obtain devices able to detect movement, typing, breathing and even speech. Continuing with CNTs, Tai *et al*. [42] developed a flexible pressure sensing film based on single wall CNT and polydimethylsiloxane spheres for human pulse signals monitoring.

Graphene derivatives have been also used for health monitoring machines. In that sense, the work carried out by Coleman and co-workers is very well known [43]. The authors published a simple method to infuse liquid-exfoliated graphene into natural rubber, obtaining strain sensors that can effectively monitor joint and muscle motion besides breathing and pulse. In a more recent work, Park and co-workers [44] have reported a smart bandage consisting of MXene-functionalized porous graphene scaffold. Thanks to the synergistic effect between graphene and MXene, the hybrid scaffold displayed high conductivity and improved electrochemistry with a fast heterogeneous electron transfer rate. These features led to the application of the final bandage for chronic wound care management, since it was able to sense uric acid, pH and temperature at the wound site. Regarding drug-delivery, a graphene-based electrochemical device with thermoresponsive microneedles for diabetes monitoring and therapy was reported [45]. The patch could be thermally activated to deliver Metformin transcutaneously, reducing blood glucose level in diabetic mice.

Perspiration from the skin gives helpful information including pH and chemical composition such as metallic ions, glucose, urea, volatile organic compounds, and so on [46], which can facilitate a prompt diagnosis of health state. In that context, interesting studies have been published. In 2013, Liao *et al*. [47] reported improved glucose sensors based on organic electrochemical transistors by incorporating graphene derivatives, achieving higher sensitivities and extending the detection limits due to the enhancement of the charge transfer and the surface to volume ratio of the gate electrode. Moreover, the authors found a negligible effect caused by uric acid an dL-ascorbic acid was observed when incorporating chitosan or Nafion. More recently, a wearable electrochemical glucose sensor was reported by Xuan *et al*. [48], based on a rGO electrode in which GO catalyzes the oxidation of glucose to glucarolactone and $H_2O_2$ by a redox reaction.

Despite the fact that some characteristics, such as the ability to shapely adapt to the rough surface of the skin, normally through van der Waals forces (tattoo-like) [49], still need to be improved in terms of thickness and modulus, the ongoing research on this kind of adherent skin-electronic devices has been highly improved in the last years [50,51], and they could map pressure, temperature or humidity distributions on the skin with high fidelity, being imperceptible by the customer and allowing even the long-term track diseases.

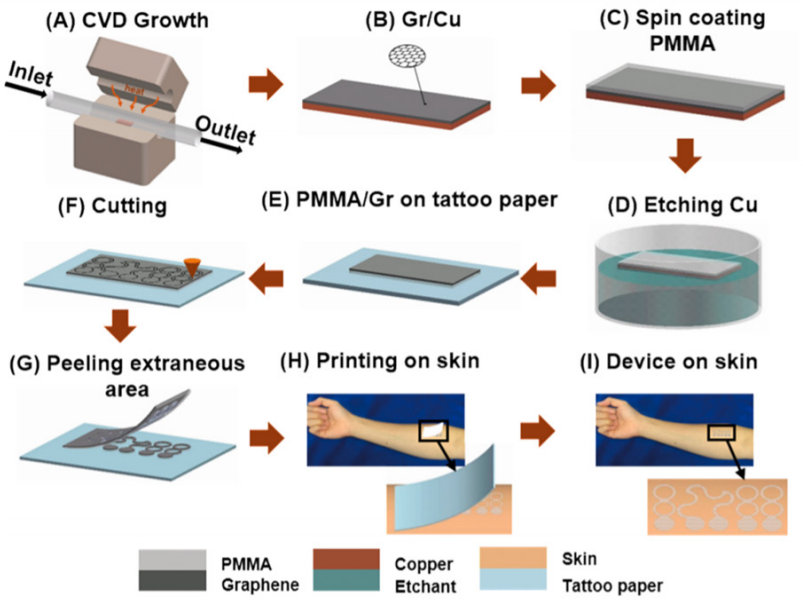


**Figure 3**. Fabrication process of a graphene electronic tattoo. Adapted with permission from [49]. Copyright 2017 American Chemical Society.

## 4. Safety and biomedical use of CBN

CBN have been described as excellent candidates with multiple applications in several sectors of society. In fact, the increasing exploitation of these nanomaterials has led to many comprehensive evaluations of their impacts on human health and environment [52–54]. In order to be aware of the possible risks on health of CBN, several works and reviews have been reported over the last few years concerning their biocompatibility and their biodegradation abilities [53,55]. Macrophages and multiple types of microbes including bacteria and fungi have the ability to degrade CNTs and graphene derivatives [56,57]. Additionally, enzymatic catalysis has been demonstrated to cause the biodegradation of single-walled CNT and other graphene-related materials using human enzymes such as eosinophil peroxidase or myeloperoxidase [58,59]. The physicochemical features of the nanomaterials play a key role on the biodegradation ability of CBN: a dispersibility-dependent biodegradation effect was found by Kurapati *et al*. [60], and chemical functionalization of the materials can enhance their degradation extent [61].

Furthermore, given the chemical nature of CBN, their dermal effects have to be taken into account: skin irritation could be considered as an important outcome after cutaneous exposure, and skin sensitization cannot be excluded in light of the tendency of CBN to interact with proteins [53]. Only a few studies reported the toxicological data and de differential effects of this kind of nanomaterials, and most of them are carried out *in vitro* on skin keratinocytes and/or fibroblasts [62]. Moreover, the conclusion about the cytotoxicity of these materials varies from one work to another, depending basically on the physicochemical properties of each specific nanomaterial such as the shape, the dimensions or the oxidative state: few-layer graphene containing almost no functional groups showed, for instance, a lower cytotoxic effect compared to GO [63]. Palmer *et al*. [64] have recently demonstrated that multi-walled CNT with a high level of carboxylation displayed increased cytotoxicity in keratinocytes compared to the multi-walled CNT with intermediate levels of carboxylation. The concentrations used for the experiments are also a key parameter regarding cytotoxicity. Tubaro and co-workers have demonstrated how keratinocytes are capable of selectively sensing low amount of graphene derivatives (concentrations up to 1 µg/mL), showing no reduction of cell viability [65]. However, adverse effects such as dermatitis or increase on protein expression due to cutaneous contact with CBN have been reported [66,67]. Due to the relevance of this topic, Fusco *et al*. [68] studied the potential of differently prepared graphene derivatives causing skin irritation using a non-animal test, SkinEthic™ Reconstructed human Epidermis. The authors concluded that graphene-based materials prepared with non-irritant exfoliation agents do not induce skin irritation after a single acute exposure.

Biomedical applications of CBN such as CNT and graphene derivatives, have been extensively studied [69,70]. Cancer therapy is maybe the most investigated area in that sense, since these nanomaterials present special physicochemical properties to load drugs on their surfaces and target them to the site of interest [71–73], as well as the possibility of using phototherapies [74]. Additionally, CNT have been demonstrated to improve transdermal drug delivery [75] and they have been also used for skin cancer diagnosis and its treatment [76,77]. Not only CNT, but of course functional GO, for instance, have been used as a plasmid-based Stat3 siRNA carrier inhibiting mouse malignant melanoma growth *in vivo* [78]. A different example could be a hybrid material based on GO and hyaluronic acid that has been used for the photothermal ablation therapy of skin cancer [79].

## 5. Conclusions

Skin is the outermost shell of the body and, because of its interfaces with the environment, skin plays a key role in protecting other organs and as a health state indicator. In this review, we introduced the use and the role of CBN for skin-related applications, focusing on CNT and graphene derivatives. Not only tactile, temperature and humidity sensors, but also devices for health monitoring and carbon nanomaterials-based hybrids for skin cancer, have been summarized across this review.

Although research on adherent skin-electronic devices has been highly improved in the last years, some features such as the capacity to shapely adapt to the rough surface of the skin still need to be improved in terms of thickness and elastic modulus to be able to map signal distributions on the skin with high fidelity, being imperceptible by the customer and allowing even the long-term track of diseases.

Despite the facts that the use of CBN for skin diseases is increasing, and also given that they have revealed to be biodegradable, the great hope raised by the inclusion of CBN in complex biological systems such as real skin constructs, remains a challenge. Therefore, this review shows that these are still emerging research areas with scientific and technical challenges requiring extensive work.

## 6. Acknowledgements

Cristina Martín acknowledges support from the CONEX-Plus programme funded by Universidad Carlos III de Madrid and the European Union's Horizon 2020 research and innovation programme under the Marie Sklodowska-Curie grant agreement No. 801538. She also acknowledges Dr José Luis Jorcano, Dr José Miguel González, Dr Amalia Ruiz and Dr Giacomo Reina for their support and advice during the writing and revision of this paper.

## 7. References

[1] Lee EK, Kim MK, Lee CH. Skin-Mountable Biosensors and Therapeutics: A Review. Annu. Rev. Biomed. Eng. 2019; 21: 299–323.

[2] Monteiro-Riviere NA, Filon FL. Effects of Engineered Nanomaterials on Skin. In: Adverse Effects of Engineered Nanomaterials: Exposure, Toxicology, and Impact on Human Health: Second Edition, Elsevier, Inc. 2017 p. 357–380.

[3] Larese Filon F, Mauro M, Adami G, Bovenzi M, Crosera M. Nanoparticles skin absorption: New aspects for a safety profile evaluation. Regul. Toxicol. Pharmacol. 2015; 72(2): 310-322.

[4] Rao N, Singh R, Bashambu L. Carbon-based nanomaterials: Synthesis and prospective applications. Mater. Today Proc. 2021; 44: 608-614.

[5] Cha C, Shin SR, Annabi N, Dokmeci MR, Khademhosseini A. Carbon-based nanomaterials: Multifunctional materials for biomedical engineering. ACS Nano 2013; 7(4): 2891–2897.

[6] Velasco D, Quílez C, Garcia M, del Cañizo JF, Jorcano JL. 3D human skin bioprinting: a view from the bio side. J. 3D Print. Med. 2018; 2(3):141–162.

[7] Wang S, Oh JY, Xu J, Tran H, Bao Z. Skin-Inspired Electronics: An Emerging Paradigm. Acc. Chem. Res. 2018; 51(5): 1033–1045.

[8] Pang C, Koo JH, Nguyen A, Caves JC, Kim MG, Chortos A, Kim K, Wang PJ, Tok JB-H, Bao Z. Highly Skin-Conformal Microhairy Sensor for Pulse Signal Amplification. Adv. Mater. 2015; 27(4): 634–640.

[9] Chen S, Jiang K, Lou Z, Chen D, Shen G. Recent Developments in Graphene-Based Tactile Sensors and E-Skins. Adv. Mater. Technol. 2018; 3(2): 1700248.

[10] Ota H, Emaminejad S, Gao Y, Zhao A, Wu E, Challa S, Chen K, Fahad HM, Jha AK, Kiriya D, Gao W, Shiraki H, Morioka K, Ferguson AR, Healy KE, Davis RW, Javey A. Application of 3D Printing for Smart Objects with Embedded Electronic Sensors and Systems. Adv. Mater. Technol. 2016; 1(1): 1600013.

[11] Lim MY, Shin H, Shin DM, Lee SS, Lee JC. Poly(vinyl alcohol) nanocomposites containing reduced graphene oxide coated with tannic acid for humidity sensor. Polymer 2016; 84: 89–98.

[12] Zhang Q, Tan L, Chen Y, Zhang T, Wang W, Liu Z, Fu L. Human□Like Sensing and Reflexes of Graphene□Based Films. Adv. Sci. 2016; 3(12): 1600130.

[13] Gong S, Schwalb W, Wang Y, Chen Y, Tang Y, Si J, Shirinzadeh B, Cheng W. A wearable and highly sensitive pressure sensor with ultrathin gold nanowires. Nat. Commun. 2014; 5(1): 1–8.

[14] Clippinger FW, Avery R, Titus BR. A sensory feedback system for an upper-limb amputation prosthesis. Bull Prosthet Res. Fall 1974; 247-58.

[15] Tang W, Yan T, Ping J, Wu J, Ying Y. Rapid Fabrication of Flexible and Stretchable Strain Sensor by Chitosan-Based Water Ink for Plants Growth Monitoring. Adv. Mater. Technol. 2017; 2(7): 1700021.

[16] Al-Handarish Y, Omisore OM, Igbe T, Han S, Li H, Du W, Zhang J, Wang L. A Survey of Tactile-Sensing Systems and Their Applications in Biomedical Engineering. Adv. Mater. Sci. Eng. 2020; 2020: 4047937.

[17] González-Domínguez JM, Martín C, Durá OJ, Merino S, Vázquez E. Smart Hybrid Graphene Hydrogels: A Study of the Different Responses to Mechanical Stretching Stimulus. ACS Appl. Mater. Interfaces 2018; 10(2): 1987–1995.

[18] Cai JH, Li J, Chen XD, Wang M. Multifunctional polydimethylsiloxane foam with multi-walled carbon nanotube and thermo-expandable microsphere for temperature sensing, microwave shielding and piezoresistive sensor. Chem. Eng. J. 2020; 393: 124805.

[19] Qi K, Zhou Y, Ou K, Dai Y, You X, Wang H, He J, Qin X, Wang R. Weavable and stretchable piezoresistive carbon nanotubes-embedded nanofiber sensing yarns for highly sensitive and multimodal wearable textile sensor. Carbon 2020; 170: 464–476.

[20] Lipomi DJ, Vosgueritchian M, Tee BC-K, Hellstrom SL, Lee JA, Fox CH, Bao Z. Skin-like pressure and strain sensors based on transparent elastic films of carbon nanotubes. Nat. Nanotechnol. 2011; 6(12): 788–792.

[21] Lou Z, Chen S, Wang L, Jiang K, Shen G. An ultra-sensitive and rapid response speed graphene pressure sensors for electronic skin and health monitoring. Nano Energy 2016; 23: 7–14.

[22] Lee S, Reuveny A, Reeder J, Lee S, Jin H, Liu Q, Yokota T, Sekitani T, Isoyama T, Abe Y, Suo Z, Someya T. A transparent bending-insensitive pressure sensor. Nat. Nanotechnol. 2016; 11(5): 472–478.

[23] Chen Z, Zhao D, Ma R, Zhang X, Rao J, Yin Y, Wang X, Yi F. Flexible temperature sensors based on carbon nanomaterials. J. Mater. Chem. B 2021; 9: 1941-1964.

[24] Yoon SG, Chang ST. Microfluidic capacitive sensors with ionic liquid electrodes and CNT/PDMS nanocomposites for simultaneous sensing of pressure and temperature. J. Mater. Chem. C 2017; 5(8): 1910–1919.

[25] Jing X, Mi HY, Peng XF, Turng LS. Biocompatible, self-healing, highly stretchable polyacrylic acid/reduced graphene oxide nanocomposite hydrogel sensors via mussel-inspired chemistry. Carbon 2018; 136: 63–72.

[26] Webb RC, Bonifas AP, Behnaz A, Zhang Y, Yu KJ, Cheng H, Shi M, Bian Z, Liu Z, Kim Y-S, Yeo W-H, Park JS, Song J, Li Y, Huang Y, Gorbach AM, Rogers JA. Ultrathin conformal devices for precise and continuous thermal characterization of human skin. Nat. Mater. 2013; 12(10): 938–944.

[27] Luo S, Liu T. SWCNT/Graphite Nanoplatelet Hybrid Thin Films for Self-Temperature-Compensated, Highly Sensitive, and Extensible Piezoresistive Sensors. Adv. Mater. 2013; 25(39): 5650–5657.

[28] Gao Z, Lou Z, Han W, Shen G. A Self-Healable Bifunctional Electronic Skin. ACS Appl. Mater. Interfaces 2020; 12(21): 24339–24347.

[29] Kenry, Yeo JC, Yu J, Shang M, Loh KP, Lim CT. Highly Flexible Graphene Oxide Nanosuspension Liquid-Based Microfluidic Tactile Sensor. Small 2016; 12(12): 1593–1604.

[30] Park J, Kim M, Lee Y, Lee HS, Ko H. Nanomaterials: Fingertip skin-inspired microstructured ferroelectric skins discriminate static/dynamic pressure and temperature stimuli. Sci. Adv. 2015; 1(9): e1500661.

[31] Zhang D, Chang H, Li P, Liu R, Xue Q. Fabrication and characterization of an ultrasensitive humidity sensor based on metal oxide/graphene hybrid nanocomposite. Sensor. Actuat. B-Chem. 2016; 225: 233–240.

[32] Lin WD, Chang HM, Wu RJ. Applied novel sensing material graphene/polypyrrole for humidity sensor. Sensor. Actuator. B-Chem. 2013; 181: 326–331.

[33] Chen Z, Lu C. Humidity sensors: A review of materials and mechanisms. Sens. Lett. 2005; 3(4): 274–295.

[34] Trung TQ, Duy LT, Ramasundaram S, Lee NE. Transparent, stretchable, and rapid-response humidity sensor for body-attachable wearable electronics. Nano Res. 2017; 10(6): 2021–2033.

[35] Sreeprasad TS, Rodriguez AA, Colston J, Graham A, Shishkin E, Pallem V, Berry V. Electron-tunneling modulation in percolating network of graphene quantum dots: Fabrication, phenomenological understanding, and humidity/pressure sensing applications. Nano Lett. 2013; 13(4): 1757–1763.

[36] Ho DH, Sun Q, Kim SY, Han JT, Kim DH, Cho JH. Stretchable and Multimodal All Graphene Electronic Skin. Adv. Mater. 2016; 28(13): 2601–2608.

[37] Kim SY, Park S, Park HW, Park DH, Jeong Y, Kim DH. Highly Sensitive and Multimodal All-Carbon Skin Sensors Capable of Simultaneously Detecting Tactile and Biological Stimuli. Adv. Mater. 2015; 27(28): 4178–4185.

[38] Khan S, Lorenzelli L, Dahiya RS. Technologies for printing sensors and electronics over large flexible substrates: A review. IEEE Sens. J. 2015; 15(6): 3164–3185.

[39] Khan S, Lorenzelli L. Recent advances of conductive nanocomposites in printed and flexible electronics. Smart Mater. Struct. 2017; 26 (8): 083001.

[40] Liu Y, Pharr M, Salvatore GA. Lab-on-Skin: A Review of Flexible and Stretchable Electronics for Wearable Health Monitoring. ACS Nano, 2017; 11(10): 9614–9635.

[41] Yamada Y, Hayamizu Y, Yamamoto Y, Yomogida Y, Izadi-Najafabadi A, Futaba DN, Hata K. A stretchable carbon nanotube strain sensor for human-motion detection. Nat. Nanotechnol. 2011; 6(5): 296–301.

[42] Tai YL, Yang ZG. Flexible pressure sensing film based on ultra-sensitive SWCNT/PDMS spheres for monitoring human pulse signals. J. Mater. Chem. B 2015; 3(27): 5436–5441.

[43] Boland CS, Khan U, Backes C, O'Neill A, McCauley J, Duane S, Shanker R, Liu Y, Jurewicz I, Dalton AB, Coleman JN. Sensitive, high-strain, high-rate bodily motion sensors based on graphene-rubber composites. ACS Nano 2014; 8(9): 8819–8830.

[44] Sharifuzzaman M, Chhetry A, Zahed MA, Yoon SH, Park CI, Zhang S, Barman SC, Sharma S, Yoon H, Park JY. Smart bandage with integrated multifunctional sensors based on MXene-functionalized porous graphene scaffold for chronic wound care management. Biosens. Bioelectron. 2020; 169: 112637.

[45] Lee H, Choi TK, Lee YB, Cho HR, Ghaffari R, Wang L, Choi HJ, Chung TD, Lu N, Hyeon T, Choi SH, Kim DH. A graphene-based electrochemical device with thermoresponsive microneedles for diabetes monitoring and therapy. Nat. Nanotechnol. 2016; 11(6): 566–572.

[46] Piro B, Mattana G, Noël V. Recent Advances in Skin Chemical Sensors. Sensors 2019; 19(20): 4376.

[47] Liao C, Zhang M, Niu L, Zheng Z, Yan F. Highly selective and sensitive glucose sensors based on organic electrochemical transistors with graphene-modified gate electrodes. J. Mater. Chem. B 2013; 1(31): 3820–3829.

[48] Xuan X, Yoon HS, Park JY. A wearable electrochemical glucose sensor based on simple and low-cost fabrication supported micro-patterned reduced graphene oxide nanocomposite electrode on flexible substrate. Biosens. Bioelectron. 2018; 109: 75–82.

[49] Ameri SK, Ho R, Jang H, Tao L, Wang Y, Wang L, Schnyer DM, Akinwande D, Lu N. Graphene Electronic Tattoo Sensors. ACS Nano 2017; 11(8): 7634–7641.

[50] Kim T, Park J, Sohn J, Cho D, Jeon S. Bioinspired, Highly Stretchable, and Conductive Dry Adhesives Based on 1D-2D Hybrid Carbon Nanocomposites for All-in-One ECG Electrodes. ACS Nano 2016; 10(4): 4770–4778.

[51] Kim DH, Lu N, Ma R, Kim YS, Kim RH, Wang S, Wu J, Won SM, Tao H, Islam A, Yu KJ, Kim T, Chowdhury R, Ying M, Xu L, Li M, Chung HJ, Keum H, McCormick M, Liu P, Zhang YW, Omenetto FG, Huang Y, Coleman T, Rogers JA. Epidermal electronics. Science 2011; 333 (6044): 838–843.

[52] Azari MR, Mohammadian Y. Comparing in vitro cytotoxicity of graphite, short multi-walled carbon nanotubes, and long multi-walled carbon nanotubes. Environ. Sci. Pollut. Res. 2020; 27(13): 15401–15406.

[53] Fadeel B, Bussy C, Merino S, Vázquez E, Flahaut E, Mouchet F, Evariste L, Gauthier L, Koivisto AJ, Vogel U, Martín C, Delogu LG, Buerki-Thurnherr T, Wick P, Beloin-Saint-Pierre D, Hischier R, Pelin M, Candotto-Carniel F, Tretiach M, Cesca F, Benfenati F, Scaini D, Ballerini L, Kostarelos K, Prato M, Bianco A. Safety Assessment of Graphene-Based Materials: Focus on Human Health and the Environment. ACS Nano 2018; 12(11): 10582–10620.

[54] Gazzi A, Fusco L, Orecchioni M, Ferrari S, Franzoni G, Yan JS Rieckher M, Peng G, Lucherelli MA, Vacchi IA, Chau NDQ, Criado A, Istif A, Mancino D, Dominguez A, Eckert H, Vázquez E, Da Ros T, Nicolussi P, Palermo V, Schumacher B, Cuniberti G, Mai Y, Clementi C, Pasquali M, Feng X, Kostarelos K, Yilmazer A, Bedognetti D, Fadeel B, Prato M, Bianco A, Delogu LG. Graphene, other carbon nanomaterials and the immune system: toward nanoimmunity-by-design. J. Phys. Mater. 2020; 3: 34009.

[55] Martín C, Kostarelos K, Prato M, Bianco A. Biocompatibility and biodegradability of 2D materials: Graphene and beyond. Chem. Commun. 2019; 55(39): 5540–5546.

[56] Chen M, Qin X, Zeng G. Biodegradation of Carbon Nanotubes, Graphene, and Their Derivatives. Trends in Biotechnol. 2017; 35(9): 836–846.

[57] Yang M, Zhang M. Biodegradation of Carbon Nanotubes by Macrophages. Front. Mater. 2019; 6: 225.

[58] Allen BL, Kichambare PD, Gou P, Vlasova II, Kapralov AA, Konduru N, Kagan VE, Star A. Biodegradation of single-walled carbon nanotubes through enzymatic catalysis. Nano Lett. 2008; 8(11): 3899–3903.

[59] Martín C, Jun G, Schurhammer R, Reina G, Chen P, Bianco A, Ménard-Moyon C. Enzymatic Degradation of Graphene Quantum Dots by Human Peroxidases. Small 2019; 15(52): 1905405.

[60] Kurapati R, Russier J, Squillaci MA, Treossi E, Ménard-Moyon C, Del Rio-Castillo AE, Vazquez E, Samorì P, Palermo V, Bianco A. Dispersibility-Dependent Biodegradation of Graphene Oxide by Myeloperoxidase. Small 2015; 11(32): 3985–3994.

[61] Ma B, Martín C, Kurapati R, Bianco A. Degradation-by-design: How chemical functionalization enhances the biodegradability and safety of 2D materials. Chem. Soc. Rev. 2020; 49(17): 6224–6247.

[62] Frontiñán-Rubio J, Gómez MV, Martín C, González-Domínguez JM, Durán-Prado M, Vázquez E. Differential effects of graphene materials on the metabolism and function of human skin cells. Nanoscale 2018; 10(24): 11604–11615.

[63] Pelin M, Fusco L, León V, Martín C, Criado A, Sosa S, Vázquez E, Tubaro A, Prato M. Differential cytotoxic effects of graphene and graphene oxide on skin keratinocytes. Sci. Rep. 2017; 7(1): 1–12.

[64] Palmer BC, Phelan-Dickenson SJ, Delouise LA. Multi-walled carbon nanotube oxidation dependent keratinocyte cytotoxicity and skin inflammation. Part. Fibre Toxicol. 2019; 16(1): 3.

[65] Fusco L, Pelin M, Mukherjee S, Keshavan S, Sosa S, Martin C, González V, Vázquez E, Prato M, Fadeel B, Tubaro A. Keratinocytes are capable of selectively sensing low amounts of graphene-based materials: Implications for cutaneous applications. Carbon 2020; 159: 598–610.

[66] Shvedova A, Castranova V, Kisin ER, Schwegler-Berry D, Murray AR, Gandelsman VZ, Maynard A, Baron P. Exposure to carbon nanotube material: Assessment of nanotube cytotoxicity using human keratinocyte cells. J. Toxicol. Environ. Heal. Part A 2003; 66(20): 1909–1926.

[67] Eedy DJ. Carbon-fibre-induced airborne irritant contact dermatitis. Contact Dermatitis 1996; 35(6): 362–363.

[68] Fusco L, Garrido M, Martín C, Sosa S, Ponti C, Centeno A, Alonso B, Zurutuza A, Vázquez E, Tubaro A, Prato M, Pelin M. Skin irritation potential of graphene-based materials using a non-animal test. Nanoscale 2020; 12(2): 610–622.

[69] Mathew T, Sree RA, Aishwarya S, Kounaina K, Patil AG, Satapathy P, Hudeda SP, More SS, Muthucheliyan K, Kumar TN, Raghu AV, Reddy KR, Zameer F. Graphene-based functional nanomaterials for biomedical and bioanalysis applications. FlatChem. 2020; 23: 100184.

[70] Maiti D, Tong X, Mou X, Yang K. Carbon-Based Nanomaterials for Biomedical Applications: A Recent Study. Front. Pharmacol. 2018; 9: 1401.

[71] Padya BS, Pandey A, Pisay M, Koteshwara KB, Hariharapura RC, Bhat KU, Biswas S, Mutalik S. Stimuli-responsive and cellular targeted nanoplatforms for multimodal therapy of skin cancer. Eur J Pharmacol. 2021; 890: 173633.

[72] Martín C, Ruiz A, Keshavan S, Reina G, Murera D, Nishina Y, Fadeel B, Bianco A. A Biodegradable Multifunctional Graphene Oxide Platform for Targeted Cancer Therapy. Adv. Funct. Mater. 2019; 29(39): 1901761.

[73] Taghavi S, Abnous K, Taghdisi SM, Ramezani M, Alibolandi M. Hybrid carbon-based materials for gene delivery in cancer therapy. J. Controlled Release 2020; 318: 158–175.

[74] Sundaram P, Abrahamse H. Phototherapy Combined with Carbon Nanomaterials (1D and 2D) and Their Applications in Cancer Therapy. Materials 2020; 13(21): 4830.

[75] Degim IT, Burgess DJ, Papadimitrakopoulos F. Carbon nanotubes for transdermal drug delivery. J. Microencapsul. 2010; 27(8): 669–681.

[76] Dianzani C, Zara GP, Maina G, Pettazzoni P, Pizzimenti S, Rossi F, Gigliotti CL, Ciamporcero ES, Daga M, Barrera G. Drug delivery nanoparticles in skin cancers. Biomed. Research Int. 2014; 2014: 895986.

[77] Siu KS, Chen D, Zheng X, Zhang X, Johnston N, Liu Y, Yuan K, Koropatnick J, Gillies ER, Min W-P. Non-covalently functionalized single-walled carbon nanotube for topical siRNA delivery into melanoma. Biomaterials 2014; 35(10): 3435–3442.

[78] Yin D, Li Y, Lin H, Guo B, Du Y, Xin Li, Jia H, Zhao X, Tang J, Zhang L. Functional graphene oxide as a plasmid-based Stat3 siRNA carrier inhibits mouse malignant melanoma growth in vivo. Nanotechnology 2013; 24(10): 105102.

[79] Jung HS, Kong WH, Sung DK, Lee MY, Beack SE, Keum DH, Kim KS, Yun SH, Hahn SK. Nanographene oxide-hyaluronic acid conjugate for photothermal ablation therapy of skin cancer. ACS Nano 2014; 8(1): 260–268.

**Dr. Cristina Martín** finished her Chemistry studies in 2012 at the University of Castilla-La Mancha (Spain) and obtained her PhD in Chemistry in 2016 from both the Universities of Trieste (Italy) and Castilla-La Mancha, working under the co-supervision of Prof. Maurizio Prato and Prof. Ester Vázquez. During her PhD studentship, she spent 3 months at the University of Brighton (UK) under the supervision of Prof. Matteo Santin. As a postdoctoral researcher she worked in 2016–2017 at IRICA (Spain). In October 2017 she joined the group of Dr Alberto Bianco as a postdoctoral fellow. Her research activities have been focused mainly on carbon nanostructures and their biodegradation and biomedical applications. Since October 2020 she is working as a CONEX-Plus Marie Curie Fellow at University Carlos III of Madrid, directing her research efforts towards the development of new approaches for wound healing through graphene-based materials.

# BlackCycle: un gran proyecto europeo para reciclar neumáticos fuera de uso en neumáticos nuevos

Michelin – Aliapur – Axelera – Ineris | Orion – Pyrum – Estato | CPERI/CERTH

CSIC – Sisener – Hera – Icamcyl | Quantis

**Coordinado por el fabricante líder mundial de neumáticos Michelin y uniendo a 7 socios industriales, 5 centros de investigación y tecnológicos (RTOs) y un cluster de innovación en un consorcio europeo en 5 países, el proyecto BlackCycle tiene como objetivo facilitar una economía circular masiva de neumáticos diseñando procesos novedosos a nivel mundial para producir neumáticos nuevos a partir de neumáticos al final de su vida útil (NFUs).**

Lanzado oficialmente en mayo de 2020, el proyecto BlackCycle involucra a 13 entidades en una alianza público-privada europea única que demostrará la viabilidad técnica, ambiental y económica de los primeros procesos circulares del mundo. El consorcio desarrollará soluciones específicas para producir materias primas sostenibles para neumáticos: recogida de NFU y selección de materias primas, optimización del proceso de pirólisis[1], valorización y refinado del líquido pirolítico, optimización del proceso de producción de negro de carbón y evaluación del rendimiento sostenible de los neumáticos. **En solo 5-6 años tras el proyecto, casi 1 de cada 2 NFUs europeos se incorporarán al único ciclo virtuoso de esta magnitud entre todos los sectores industriales para la recuperación de productos al final de su vida útil.**

Financiado por el programa Horizonte 2020, BlackCycle se beneficia de un presupuesto general de aproximadamente 16 M € con una financiación europea asignada de aproximadamente 12 M € (75% de los costos del proyecto, ver Fig.1). Un 35% de la financiación del proyecto se asigna a PYMEs, un 15% a RTOs y un 34% corresponde a costes de personal. El consorcio cubre 5 países europeos: Francia, España, Alemania, Grecia y Suiza e incluye 7 socios industriales, 5 RTOs y un cluster de innovación. Coordinado por Michelin, el consorcio ha diseñado un sistema de gobernanza eficaz que incluye un comité directivo, un consejo de sinergias de clústeres y un comité de soporte técnico.

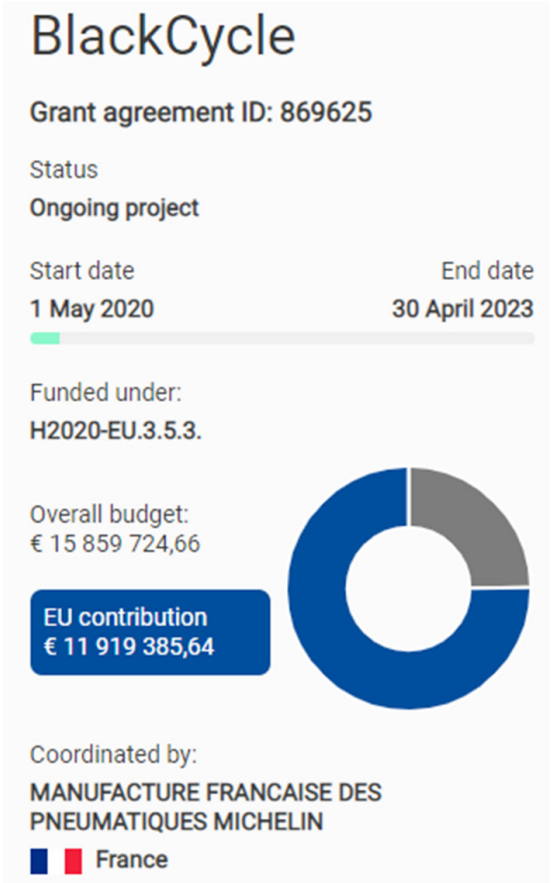


**Figura 1**. Información del proyecto BlackCycle. (Fuente Cordis).

## Contexto

Cada año se venden 1.600 millones de neumáticos nuevos en todo el mundo, lo que representa más de 26 millones de toneladas, y el mismo volumen llega a la categoría de neumáticos al final de su vida útil (NFU), lo que proporciona un gran y solo parcialmente aprovechado potencial para la recuperación de materiales. Los procesos de tratamiento de NFUs hoy no son circulares y no dan como resultado materias primas que puedan reutilizarse en la industria del neumático. Además, al no existir una solución adecuada para valorizar los materiales de NFU en la UE, más de la mitad de los neumáticos al final de su vida útil y de segunda mano de la UE se exportan a países en desarrollo.

## Objetivo: Una economía circular de neumáticos en Europa

El proyecto BlackCycle tiene como objetivo crear, desarrollar y optimizar una cadena de valor completa desde la materia prima NFU hasta las materias primas secundarias (SRM), sin desperdicio de recursos en ninguna parte de la cadena y con una atención específica al impacto ambiental. Estos SRM se utilizarán para desarrollar nuevas gamas de neumáticos para automóviles y camiones, que se venderán comercialmente en los mercados europeos y mundiales. **Como resultado, la cadena de valor BlackCycle tiene una menor huella de carbono (ver Imagen 2), emitiendo 0,93 kg / CO2 / kg de neumático y con un menor uso de**

**recursos fósiles, utilizando 0,89 kg materiales fósiles / kg NFU.**

Al ofrecer una alternativa económica y ambientalmente viable, BlackCycle reducirá la exportación de neumáticos al final de su vida útil. Al reubicar la gestión y transformación de neumáticos al final de su vida útil dentro de la UE, se espera que BlackCycle cree empleos sostenibles dentro de la UE.


**Figura 2**. Comparación de la Huella de Carbón entre procesos de producción.

**Michelin**
Hervé Erschler | Press Relations Michelin Group
+33 670 478 504
*herve.erschler@michelin.com*

**Orion Engineered Carbons**
Dirk Rechenbach | Vice President Marketing Business Line Rubber
+49 151 120 28 200
*dirk.rechenbach@orioncarbons.com*

**Pyrum Innovations**
Pascal Klein | MBA
+49 6831 95948 0
*pascal.klein@pyrum.net*

**Quantis**
Christina Papadimitriou | Sustainability Consultant
+41 21 3535 910
*christina.papadimitriou@quantis-intl.com*

**CSIC-Instituto de Carboquimica (ICB)**
Ramon Murillo | Scientific Researcher and leader of the Environmental Research Group
+34 976 733 977
*ramon.murillo@csic.es*

**CPERI/CERTH**
Elli Heracleous | Associate Professor
+30 2310 498 345
*eheracle@certh.gr*

**Sisener Ingenieros SL**
Pablo Gonzalez | Thermal Department Manager
+34 91 658 68 38
*pgonzalez@sisener.com*

**Aliapur**
Stéphanie Lafond | Communication Director
+33 6144 815 42
*slafond@aliapur.fr*

**Estato Umweltservice GmbH**
Alexander Prokein | CEO
+49 9613 065 227
*Alexander.Prokein@estato-umweltservice.de*

**HERA Holding**
Javier Lacoma | International Business Manager
+34 932 051 010
*javier.lacoma@heraholding.com*

**AXELERA**
Laura-Mia Grevon | Communication & Event manager
+33 772 006 789
*laura.grevon@axelera.org*

**Ineris**
Karine Grimault | Press & media relations officer
+33 649 334 960
*Karine.GRIMAULT@ineris.fr*

**Fundacion ICAMCYL**
Santiago Cuesta | General Director
+34 987 440 481
*comunicacion@icamcyl.com*

# Socios protectores del Grupo Español del carbón

Industrial Química del Nalón, S.A.
NalónChem